

INFRARED IMAGING AND OPTICAL IMAGING AND SPECTROSCOPY OF (MOSTLY) TYPE I PLANETARY NEBULAE. I.¹

J. Bohigas

Instituto de Astronomía
Universidad Nacional Autónoma de México
Received 2001 May 21; accepted 2001 September 6

RESUMEN

Se presenta información espectroscópica, imágenes en las principales líneas ópticas de emisión e imágenes infrarojas para descubrir la presencia de hidrógeno molecular, de 14 nebulosas planetarias (NPs). Nueve de ellas satisfacen los dos criterios que definen a las NPs de tipo I (ricas en helio con un alto cociente de N/O). Todas éstas son bipolares y, excepto Sh 2–71, muestran H₂ chocado. La composición química de JnEr 1 implica que fue producida por una progenitora masiva y puede ser tentativamente clasificada como de tipo I. A 26 es una NP elíptica rica en helio, con un bajo cociente de N/O y probablemente sin H₂. Se encontró hidrógeno molecular chocado en K 3–92, una NP elíptica de tipo IIb, lo que significa que este objeto es probablemente joven. La composición química de K 3–72, K 4–55, M 1–75 y Sh 2–71 indica que se produjeron episodios de tercer dragado en su estrella progenitora. Las temperaturas y propiedades espectrales de BV 5–1, K 4–55, M 1–41, M 1–75 y Sh 2–71 sugieren la existencia de ondas de choque en su componente ionizada.

ABSTRACT

Optical spectra, images in the main optical emission lines and IR images directed towards the detection of molecular hydrogen, were obtained for 14 planetary nebulae (PNe). It was found that nine of these comply with the two criteria defining a type I PNe (He-rich with a large N/O ratio). All of these objects are bipolar and, with the exception of Sh 2–71, show shocked molecular hydrogen. The chemical composition of JnEr 1 indicates it was produced by a massive progenitor, and it can be tentatively classified as a type I PN. A 26 is a helium rich elliptical with a low N/O abundance ratio, probably without H₂. Shocked H₂ was found in K 3–92, an elliptical type IIb, which implies that this object is probably young. The chemical composition of K 3–72, K 4–55, M 1–75, and Sh 2–71 indicate that third dredge-up episodes occurred in their progenitor star. The temperatures and spectral properties of BV 5–1, K 4–55, M 1–41, M 1–75, and Sh 2–71 suggest the presence of shock waves in their ionized component.

Key Words: ISM: ABUNDANCES — ISM: INDIVIDUAL (BV 5–1: JNER 1: K 3–72: M 1–41: M 2–53: SH 2–71) — PLANETARY NEBULAE

1. INTRODUCTION

The largest helium and nitrogen abundances observed in planetary nebulae (PNe) occur in those classified as type I, where $\text{He}/\text{H} \geq 0.125$ and $\text{N}/\text{O} \geq 0.5$ (Peimbert & Torres-Peimbert 1983).

These large abundances are a consequence of nuclear processed material being dredged-up to the stellar envelope (Iben 1995) in the early asymptotic giant branch (AGB) phase and, in some cases, during the thermally pulsating AGB phase (leading to extreme He/H, N/O, and C/O ratios, plus Ne and s-process elements), which implies that type I PNe are the end product of the most massive stars producing

¹Based on observations collected at the Observatorio Astronómico Nacional in San Pedro Mártir, B. C., México.

PNe, between ~ 2.4 and $8 M_{\odot}$ when in main sequence. Evolutionary models for the central stars of PNe (PNN or post-AGB stars) predict that higher ZAMS masses for the central star lead to more massive PNN, and hotter, more accelerated and more luminous post-AGB evolutionary tracks (Schönberner 1981; Vassiliadis & Wood 1994; Blöcker 1995). Various authors have confirmed that, in general, central stars of type I PNe lie on higher mass tracks than the PNN of other types of PNe (e.g., Kaler 1983a; Pottasch 1983; Stasińska & Tylenda 1990). Considering that type I PNe should have a mass of at least $1.5 M_{\odot}$ and maybe as much as $7 M_{\odot}$ (see Iben 1995, Fig. 21), and that $\sim 20\%$ of all PNe are of this type, it follows that a substantial contribution to the He and N enrichment of the interstellar medium is due to type I PNe (Peimbert 1987).

It is probable that all type I PNe have a bipolar structure. The magnetic field of a rotating central star can generate a bipolar nebula (Różyczka & Franco 1996; García-Segura et al. 1998), but it is generally believed that this morphology is caused by a high density torus confining the fast low-density wind of the PNN (Kwok 1982; Kahn 1983; Balick 1987). The toroid is thought to be an equatorial density enhancement in the slow massive wind (the *superwind*) produced by the star while in the AGB phase (though most AGB stars are spherical, e.g., Sahai & Biegging 1993). The optical spectra of type I PNe are characterized by the presence of forbidden lines from high and low ionization species (from [O I] to [Ne V] or more), and in many objects the intensity of these lines is comparable to the intensity of the H-Balmer lines. The presence of strong lines from low ionization species indicates that type I PNe spend most of their lifetime being optically thick (Sabbadin 1986). It has also been proposed that the large strength of forbidden lines may be caused by shock waves resulting from the interaction between the fast outflow of the PNN and the material deposited by the *superwind* (e.g., Phillips 1998). Line ratio images of NGC 6302 are a particularly nice example of the possible importance of shock waves in these objects (Bohigas 1994, 1998). Phillips & Guzmán (1998), upon examining the relative roles of radiative and collisional excitation, concluded that spectral deviations associated to shock waves are more likely to occur in bipolar nebulae. These deviations can lead to inappropriate abundance determinations (Peimbert, Sarmiento, & Fierro 1991), since the intensity of forbidden lines is enhanced with respect to a situation where the plasma is only subject to photoionization.

In order to further explore the properties of type I PNe optical spectra, images in the main optical emission lines, and IR images directed towards the detection of molecular hydrogen were obtained for nearly 30 PNe. There is little or fragmentary information for most of these objects, which were chosen from the *Strasbourg-ESO Catalogue of Planetary Nebulae* (Acker et al. 1992) based on relatively large intensities of [N II] 6584 and/or [S II] 6717,6731 with respect to H α . Results for the following 14 planetary nebulae are presented in this paper: A 26, BV 5–1, HDW 5, JnEr 1, K 3–72, K 3–92, K 3–94, K 4–55, M 1–41, M 1–75, M 2–52, M 2–53, Sh 2–71, and We 1–4. The remaining objects will be discussed in a forthcoming publication. This paper is organized as follows: the experimental setup and data reduction procedures are described in § 2, observations are discussed in some detail in § 3, and the last section summarizes the most significant findings.

2. OBSERVATIONS AND DATA REDUCTION

2.1. Optical Imaging

Images with narrow band filters centered at H β , [O III] 5007, H α , [N II] 6584, and [S II] 6724 were obtained for most of the objects discussed in this paper. Observations with filters centered at [N II] 5755 and [S II] 6731 were also made in Sh 2–71. The SPM set of nebular filters (series I and II) was used. Filter properties can be found at <http://bufadora.astro.unam.mx/Instruments/filtros/filtros.html>. Images were secured during several observing runs, using the three telescopes at the Observatorio Astronómico Nacional at San Pedro Mártir, B. C., México (OAN) and various CCD detectors. The 2.1 m observations were carried out with the f/7.5 secondary. The *RUCA* filter wheel (Zazueta et al. 2000) was used in the 1.5 and 0.84 m telescope observations. Integration times were typically 20 minutes, and up to 60 minutes for weak lines or deep observations. Sky flats were used in all these runs. Image quality was rarely better than $1.3''$.

The H α images were used to determine the total H α flux from each object. A “pure” H α image was produced removing (i.e., forcing a zero value) all stars and pixels where the number of counts was $\leq 3\sigma$ above the mean sky level (where no source emission is found). Image counts were then converted into flux units using a scaling factor derived from the spectral data described in the next section. The H β flux obtained from the spectroscopy is precise at the 10% level. The slit central position was determined by matching profiles from several images with the corresponding lines in the spectrum. Posi-

tioning errors are within $2''$. An additional source of uncertainty in the reported $H\alpha$ fluxes for the largest PNe is the accuracy of flat fielding, but this is probably a minor effect since all spectra were taken at or very near the brightest regions.

Images of these objects in some of the emission lines explored in this work have been reported in a number of contributions, among them *The IAC Morphological Catalog of Northern Galactic Planetary Nebulae* (Manchado et al. 1996, henceforth IAC-Catalog), to which reference is made on several occasions.

2.2. IR Imaging

Infrared images were obtained with the $H2$ ($\lambda_0 = 2.122 \mu\text{m}$, FWHM = $0.02 \mu\text{m}$) and cK ($\lambda_0 = 2.26 \mu\text{m}$, FWHM = $0.06 \mu\text{m}$) filters of the CAMILA imaging system (Cruz-González et al. 1994) attached to the 2.1 m f/13.5 telescope of the OAN. The field of view of the detector, a NICMOS3 256×256 pixel² infrared camera, is $218'' \times 218''$. Image quality is 2–3 pixel in all cases. Typical total integration times were 900 s for $H2$, and 600 s for cK . Most objects are completely included in a quadrant of the detector, and were rastered to different locations within it. In these cases the sky frame is the median of all images in the sequence (more than 9). For large objects the sky frame was produced from images in the immediate vicinity. Flat fields are the median of all night frames for each filter. Since detection and morphology was the main goal in the IR band, the images were not photometrically calibrated.

The filter identified as $H2$ is centered at the wavelength of the H_2 1–0 S(1) transition at $2.1213 \mu\text{m}$ (air). The cK filter is used to determine if there is emission from the continuum and/or the H_2 2–1 S(1) transition at $2.2471 \mu\text{m}$ (air). The nature of the emitting gas can be established assuming that no other emission lines fall within the transmission curves of these filters (which is not the case, see below). The relative strength of these two H_2 lines determines whether molecular hydrogen emission is produced by radiative excitation in photodissociation regions or by shock waves, as long as the density $\leq 10^5 \text{ cm}^{-3}$: shock excited regions give a value ~ 10 for the 2.1213 to $2.2471 \mu\text{m}$ intensity ratio, while in fluorescent emission this ratio is closer to 2 (Burton 1992). For larger densities radiative excitation yields larger ratios, and the exciting mechanism cannot be established unambiguously with these two lines only. Thus, shock excitation can be taken as a working hypothesis when there is extended emission in the $H2$ image, but there is none (or very faint) in the cK frame. An $H2 - cK$ image was produced

when extended emission was detected with both filters, matching the background and the star counts on each pair of source frames. It is assumed that extended emission is due to the continuum when no residual emission is left. Otherwise, relative intensities must be inspected in order to assess which is the most likely mechanism exciting H_2 emission (if the presence of molecular gas is suspected).

The cK filter includes other H_2 transitions besides the one at $2.2471 \mu\text{m}$, as well as faint CO lines and an unidentified and sometimes strong line at $2.28 \mu\text{m}$ (see Hora, Latter, & Deutsch 1999). More importantly (and unfortunately), the $H2$ filter also includes a He I doublet at $2.11 \mu\text{m}$, since its transmission is $\sim 20\%$ at this wavelength (60% at $2.12 \mu\text{m}$). These lines have been observed in many PNe (e.g., Luhman & Rieke 1996; Hora et al. 1999). This implies that conclusions on the presence of H_2 based only on the preceding arguments cannot be regarded as definitive. Spectral observations, imaging with a narrower filter centered at the H_2 transition at $2.12 \mu\text{m}$, or images with filters centered at other He I lines (such as He I 5876) are required to do so. On the other hand, in the absence of other evidence, it can be presumed that molecular gas is probably dominant if emission is concentrated on an equatorial region, or if it is seen in a bipolar nebula (Zuckerman & Gatley 1988; Latter et al. 1995; Kastner et al. 1996). If neither of these conditions is fulfilled, it is more likely that emission is being dominated by the He I lines at $2.11 \mu\text{m}$ (Hora et al. 1999).

Emission through the $H2$ filter was detected in all the objects included in this sample. Extended but very faint emission is observed through the cK filter in four of these objects (K 3–72, K 3–92, K 3–94, and M 2–53). No image of HDW 5 could be obtained with the cK filter, though the object is very bright and similar to other PNe when seen through the $H2$ filter. Shocked molecular hydrogen is probably associated to BV 5–1, K 3–72, K 3–94, K 4–55, M 1–41, M 1–75, M 2–52, and We 1–4. Finally, emission through a similar $H2$ filter from four of these objects (BV 5–1, K 4–55, M 1–75, and M 2–52) was reported by Guerrero et al. (2000) while this work was in progress.

2.3. Optical Spectroscopy

Spectroscopy was carried out with the Boller & Chivens spectrograph at the 2.1 m f/7.5 telescope of the OAN. A 600 lines mm^{-1} grating blazed at 4550 \AA was used to cover the 3700–5300 and 4750–6850 \AA wavelength intervals. In eight cases a 600

TABLE 1
SPECTRAL POSITIONS

Object	Name	GSC	$\Delta\alpha$	$\Delta\delta$	P.A.	Other ^a
G250.3+00.1	A 26	7125-01450	75''	-92''	NS	...
G119.3+00.3	BV 5-1	4019-01364	-37''	-31''	NS	KCJ
G218.9-10.7	HDW 5	5368-01056	-91''	9''	EW	AP
G164.8+31.1	JnEr 1	3783-00629	22''	33''	NS	...
G204.8-03.5	K 3-72	0141-00257	65''	-11''	EW	...
G130.4+03.1	K 3-92	4041-00305	3''	-89''	EW	KSK
G142.1+03.4	K 3-94	4062-01451	48''	129''	EW	KKSB
G084.2+01.1	K 4-55	3178-00319	-35''	45''	NS	GMS
G006.7-02.2	M 1-41	6843-00239	-74''	-65''	NS	D, AKSR
G068.8-00.0	M 1-75	2670-02070	-3''	42''	EW	AK, GSM
G103.7+00.4	M 2-52	3990-00695	37''	95''	NS	KKSB
G104.4-01.6	M 2-53	3987-01879	-102''	45''	NS	KSK
G035.9-01.1	Sh 2-71 E	0466-02019	10''	0''	EW	SFO
G035.9-01.1	Sh 2-71 NE	0466-02019	21''	24''	NS	SFO
G201.9-04.6	We 1-4	0730-01427	-106''	90''	EW	...

^aOther spectroscopic work by: AP: Ali & Pfeleiderer 1999. AK: Aller & Keyes 1987. AKSR: Acker et al. 1991. D: Dopita 1977. GMS: Guerrero et al. 1996. GSM: Guerrero et al. 1995. KCJ: Kaler et al. 1988. KKSB: Kaler et al. 1996. KSK: Kaler et al. 1990. SFO: Sabbadin et al. 1987.

lines mm^{-1} grating blazed at 6825 \AA was used to cover the $6600\text{--}8700 \text{ \AA}$ wavelength interval. The slit was $250 \mu\text{m}$ wide and its alignment varied from object to object (see Table 1). The mean spectral resolution and dispersion are ~ 3 pixel and $2.05 \text{ \AA}/\text{pixel}$ respectively (the pixel size is $24 \mu\text{m}$). Most exposures were 20 minutes long. Flux calibration was performed and crosschecked using several standard stars.

Data reduction was performed applying IRAF² standard procedures. Most extraction apertures are $5'' \times 3''$ (length and width of the slit). To obtain a higher signal to noise ratio, a larger aperture was used for A 26 and We 1-4 (see Table 2). Sky spectra were extracted from the same frame as the object spectra. The positions at which the latter were obtained (accurate within $2''$) are annotated in Table 1, and are given in relation to stars from the *Hubble Guide Star Catalogue* (also listed in this table). These positions are marked in one of the optical images of each object (Figures 1 to 16). References to previous spectroscopic observations are also included in Table 1 (under Other).

²IRAF is distributed by NOAO which is operated by AURA under contract to the NSF.

Line fluxes relative to $\text{H}\beta$ (100 in all cases) are reported in Table 2. Errors in the $\text{H}\beta$ fluxes are always smaller than 15%. The red spectrum was scaled using the [S II] 6717,6731 lines. Reddening corrections were performed with Seaton's (1979) extinction law assuming that $\text{H}\alpha/\text{H}\beta = 2.8$. Electron densities and temperatures were determined using the *nebular* package from the Space Telescope Science Data Analysis System. These parameters are given in Table 3. The S^+ lines are very well defined in all cases, and ratios are probably precise at the $\sim 5\%$ level. Temperatures ($T(\text{O}^{+2})$ and $T(\text{N}^+)$) were determined from the $R(\text{O}^{+2}) = [\text{O III}] (4959+5007)/4363$ and $R(\text{N}^+) = [\text{N II}] (6548+6584)/5755$ line ratios. Upper and lower bounds for the nitrogen and oxygen temperatures were determined assuming that the corresponding line ratios are uncertain at the 10% level when the flux of the weakest line involved in the ratio ([N II] 5755 or [O III] 4363) is larger than $5 \times 10^{-16} \text{ erg cm}^{-2} \text{ s}^{-1}$, and at the 20% level when smaller than this quantity.

Ion abundances are presented in Table 4. The abundance of helium ions was calculated following Aller (1984). Collisional effects on the He I lines were always considered when determining the He^+

TABLE 2
SPECTRAL RESULTS ($H\beta = 100$)

ID	A 26 ^d		BV 5-1		HDW 5		JnEr 1		K 3-72	
	F_λ	I_λ	F_λ	I_λ	F_λ	I_λ	F_λ	I_λ	F_λ	I_λ
[O II] 3727			216	373	556	933	687	806	82.1	180
[Ne III] 3869			107	171			103	118	40.2	74.1
H δ			18.7	26.6	17.9	25.1	22.5	25.0	15.8	25.1
H γ	33.4	52.4	38.1	49.6	41.6	53.5	53.5	57.8	34.1	48.1
[O III] 4363			20.0	25.8			5.10	5.49	1.81	2.52
He I 4471			5.14	6.24	3.05	3.68	4.92	5.21	4.26	5.48
He II 4686			62.0	67.4			22.4	22.9	23.8	26.5
[Ar IV] 4711 ^a			7.24	7.78						
[Ar IV] 4740			3.70	3.91						
[O III] 4959	249	230	332	317	10.7	10.3	230	227	129	121
[O III] 5007	769	683	1012	944	33.0	30.9	733	719	409	373
[N I] 5200			22.0	18.9	5.64	4.92	5.02	4.80	37.3	30.7
[Cl III] 5518			3.35	2.52						
[Cl III] 5538			2.13	1.59						
[N II] 5755	12.7	6.50	37.5	25.4	3.95	2.74	8.74	7.79	33.3	20.0
He I 5876	40.7	19.1	23.9	15.4	19.1	12.6	21.5	18.9	31.3	17.6
[O I] 6300			73.6	41.0	38.8	22.4	31.4	26.5	32.3	15.1
[S III] 6312			12.5	6.94					3.69	1.71
[O I] 6364			25.2	13.8	12.7	7.22	11.8	9.88	9.82	4.47
[Ar V] 6435			2.05	1.11						
[N II] 6548	306	99.2	654	339	102	55.1	238	196	1361	578
H α										
[N II] 6548	306	99.2	654	339	102	55.1	238	196	1361	578
H α	866	280	542	280	522	280	340	280	665	280
[N II] 6584	900	288	2063	1060	320	171	742	611	4233	1776
He I 6678	16.5	5.07	8.81	4.41	6.06	3.16			10.4	4.22
[S II] 6717	100	30.1	186	92.1	120	62.0	19.4	15.8	90.2	36.1
[S II] 6731	73.0	21.8	179	88.3	95.5	49.2	13.5	11.0	72.9	29.0
[Ar V] 7006			4.19	1.94						
He I 7065			11.0	5.02						
[Ar III] 7136	72.3	18.4	91.5	41.1			33.9	26.8		
He II 7178			3.59	1.61						
[O II] 7320	44.5	10.6								
[O II] 7331	39.3	9.33	19.1	8.21						
[Ar III] 7751			24.7	9.80						
$F(H\beta)^b$	1.14		2.17		2.04		0.58		1.73	
$C(H\beta)$	1.52		0.89		0.84		0.26		1.16	
$I(H\beta)^c$		3.75		1.68		1.40		0.11		2.52

^a Blend [Ar IV] 4711, He I 4713, and [Ne IV] 4715. ^b $F(H\beta)$ in 10^{-14} erg cm⁻² s⁻¹.

^c $I(H\beta)$ in 10^{-13} erg cm⁻² s⁻¹. ^d A 26 aperture is 29'' long.

TABLE 2 (CONTINUED)

ID	K 3-92		K 3-94		K 4-55		M 1-41		M 1-75	
	F_λ	I_λ	F_λ	I_λ	F_λ	I_λ	F_λ	I_λ	F_λ	I_λ
[O II] 3727	271	664	287	408	71.1	199	85.9	302		
[Ne III] 3869	54.4	117	75.7	102	52.1	127	35.9	106	54.8	215
H δ	14.5	25.9	21.5	27.0			11.4	25.9	9.22	25.8
H γ	31.3	48.4	41.0	48.7	30.4	50.3	25.5	47.0	24.3	52.5
[O III] 4363	6.43	9.83	14.1	16.6	11.4	18.4	9.78	17.6	13.5	28.3
He I 4471										
He II 4686	5.89	6.77	35.1	37.0	50.4	59.2	44.1	53.7	80.8	103
[Ar IV] 4711 ^a					13.3	15.3	8.28	9.82	13.7	17.0
[Ar IV] 4740					7.38	8.19	6.12	6.96	11.0	12.9
[O III] 4959	319	296	285	277	301	276	231	207	656	572
[O III] 5007	1089	974	858	820	901	790	763	650	2034	1660
[N I] 5200	4.56	3.57	18.8	17.1	20.4	15.3	31.5	22.1	32.3	20.9
[Cl III] 5518										
[Cl III] 5538									8.22	3.49
[N II] 5755	8.18	4.31	13.7	10.7	47.2	22.5	62.4	25.2	55.5	17.7
He I 5876	31.3	15.2	20.0	15.0	34.9	15.1	36.8	13.2	33.8	9.10
[O I] 6300	80.9	31.1	134	92.0	67.3	22.2	161	41.5	147	26.8
[S III] 6312			3.79	2.67	23.5	7.70	28.8	7.36	37.8	6.79
[OI] 6364	24.5	9.11	35.2	23.9	20.1	6.43	53.0	13.2	40.0	6.90
[Ar V] 6435						-	5.31	1.28	4.79	0.80
[N II] 6548	220	74.8	243	159	1194	343	1662	362	2771	407
H α	830	280	429	280	981	280	1294	280	1931	280
[N II] 6584	733	246	751	490	4027	1138	4464	954	8275	1185
He I 6678	9.55	3.07	8.22	5.27	17.3	4.64	16.8	3.38	19.6	2.59
[S II] 6717	90.4	28.6	67.4	42.9	198	52.2	233	45.8	486	62.5
[S II] 6731	75.6	23.8	57.0	36.2	202	52.8	320	62.2	517	65.7
[Ar V] 7006			3.12	1.97			32.5	5.46	11.0	1.16
He I 7065			6.71	4.21	16.5	3.72	34.1	5.56	25.5	2.58
[Ar III] 7136			30.5	18.9	125	27.3	371	58.2	370	35.7
He II 7178										
[O II] 7320			14.9	9.03	24.7	5.01	143	20.5	54.5	4.69
[O II] 7331			11.4	6.92	21.1	4.26	93.3	13.4	44.3	3.79
[Ar III] 7751			6.97	4.02	41.6	7.19	142	16.8	126	8.46
$F(\text{H}\beta)^b$	1.01		0.36		0.59		2.39		0.50	
$C(\text{H}\beta)$	1.46		0.57		1.69		2.06		2.60	
$I(\text{H}\beta)^c$		2.92		0.14		2.88		27.3		19.6

^a Blend [Ar IV] 4711, He I 4713, and [Ne IV] 4715. ^b $F(\text{H}\beta)$ in 10^{-14} erg cm⁻² s⁻¹.^c $I(\text{H}\beta)$ in 10^{-13} erg cm⁻² s⁻¹.

TABLE 2 (CONTINUED)

ID	M 2-52		M 2-53		Sh 2-71 E		Sh 2-71 NE		We 1-4 ^d	
	F_λ	I_λ	F_λ	I_λ	F_λ	I_λ	F_λ	I_λ	F_λ	I_λ
[O II] 3727	129	325	253	413	119	191	257	437		
[Ne III] 3869	76.8	168	71.2	109	93.3	140	116	183		
H δ	16.5	29.8	19.7	27.1	18.0	24.4	18.7	26.4		
H γ	30.1	46.9	35.7	45.2	35.6	44.8	34.7	44.9	33.7	45.3
[O III] 4363	14.7	22.5	7.19	9.04	17.7	22.1	13.2	16.9		
He I 4471	3.27	4.54	6.39	7.62						
He II 4686	54.8	63.2	18.4	19.9	85.2	91.6	52.7	57.2	32.2	35.5
[Ar IV] 4711 ^a	6.01	6.80			13.8	14.7				
[Ar IV] 4740	3.33	3.65			7.81	8.19				
[O III] 4959	408	378	298	286	284	273	272	260	91.1	86.4
[O III] 5007	1272	1133	932	876	878	827	846	790	297	275
[N I] 5200	15.5	12.0	7.01	6.12	27.2	23.8	17.6	15.2	25.9	21.9
[Cl III] 5518	3.24	2.01	0.92	0.71						
[Cl III] 5538	2.94	1.80	1.53	1.18						
[N II] 5755	41.6	21.6	8.17	5.75	45.3	32.3	67.1	45.8	40.3	26.1
He I 5876	23.4	11.1	19.5	13.1	22.4	15.3	28.0	18.2	45.4	27.7
[O I] 6300	44.9	16.9	44.5	26.3	39.4	23.7	33.8	19.1	65.1	33.9
[S III] 6312	18.7	6.96	1.96	1.16	15.0	9.01	15.4	8.68		
[O I] 6364	15.5	5.63	15.1	8.79	13.6	8.06	14.0	7.78	25.0	12.7
[Ar V] 6435	1.72	0.61								
[N II] 6548	925	307	214	118	846	478	1307	688	801	384
H α	848	280	506	280	497	280	534	280	586	280
[N II] 6584	2853	934	661	363	2663	1494	4111	2147	2579	1226
He I 6678	9.14	2.86	7.58	4.07	11.5	6.31	13.4	6.82	10.8	5.00
[S II] 6717	163	50.1	55.7	29.6	180	97.8	249	125	87.2	39.8
[S II] 6731	180	54.9	53.5	28.3	172	93.2	207	104	59.9	27.2
[Ar V] 7006			4.25	2.18						
He I 7065					8.14	4.13	9.90	5.03		
[Ar III] 7136					108	54.0	81.3	37.2		
He II 7178										
[O II] 7320					24.9	12.0	17.5	7.70		
[O II] 7331					17.8	8.59	16.0	7.02		
[Ar III] 7751					35.6	16.0	25.1	10.2		
$F(\text{H}\beta)$ ^b	2.61		4.34		0.98		1.05		0.71	
$C(\text{H}\beta)$	1.49		0.80		0.77		0.87		0.99	
$I(\text{H}\beta)$ ^c		8.07		2.74		0.58		0.78		0.70

^a Blend [Ar IV] 4711, He I 4713, and [Ne IV] 4715. ^b $F(\text{H}\beta)$ in 10^{-14} erg cm⁻² s⁻¹.^c $I(\text{H}\beta)$ in 10^{-13} erg cm⁻² s⁻¹. ^d We 1-4 aperture is 27'' long.

TABLE 3
DENSITY AND TEMPERATURE

Object	$R([\text{S II}])^a$	N_e	$R([\text{N II}])$	$T_e (\text{N}^+)$	$R([\text{O III}])^b$	$T_e (\text{O}^{+2})$
A 26	1.38±0.07	35 $^{+70}_{-35}$	59.6±5.96	12600 $^{+700}_{-600}$		
BV 5-1	1.04±0.05	540 $^{+130}_{-110}$	55.1±5.51	12000 $^{+700}_{-500}$	48.9±4.89	17800 $^{+1000}_{-900}$
HDW 5	1.26±0.06	170 $^{+70}_{-70}$	82.5±8.52	10800 $^{+500}_{-400}$		
JnEr 1	1.44±0.07	≤ 10	104±20.8	9800 $^{+1000}_{-600}$	172±34.8	10600 $^{+900}_{-600}$
K 3-72	1.24±0.06	185 $^{+75}_{-65}$	118±11.8	9300 $^{+400}_{-300}$	196±39.2	10200 $^{+700}_{-500}$
K 3-92	1.20±0.06	245 $^{+95}_{-80}$	74.4±7.44	11300 $^{+300}_{-500}$	129±12.9	11700 $^{+500}_{-400}$
K 3-94	1.19±0.06	265 $^{+100}_{-85}$	60.4±12.1	12500 $^{+1500}_{-1100}$	66.1±13.2	15300 $^{+1800}_{-1200}$
K 4-55	0.99±0.05	670 $^{+150}_{-130}$	65.9±6.59	11800 $^{+700}_{-500}$	57.9±5.79	16300 $^{+900}_{-700}$
M 1-41	0.74±0.04	2060 $^{+410}_{-380}$	52.3±5.23	13000 $^{+700}_{-700}$	48.6±4.86	17800 $^{+1100}_{-800}$
M 1-75	0.95±0.05	750 $^{+170}_{-140}$	89.9±8.99	10300 $^{+500}_{-400}$	78.9±7.89	14200 $^{+600}_{-600}$
M 2-52	0.91±0.05	950 $^{+220}_{-170}$	57.5±5.75	12600 $^{+700}_{-600}$	67.0±6.70	15200 $^{+800}_{-600}$
M 2-53	1.05±0.05	480 $^{+120}_{-90}$	83.7±8.37	10000 $^{+400}_{-400}$	129±12.9	11700 $^{+500}_{-400}$
Sh 2-71 E	1.05±0.05	500 $^{+130}_{-90}$	61.1±6.11	11400 $^{+600}_{-500}$	49.8±4.98	17600 $^{+1000}_{-800}$
Sh 2-71 NE	1.20±0.06	260 $^{+90}_{-80}$	61.9±6.19	11400 $^{+600}_{-500}$	62.1±6.21	15700 $^{+900}_{-600}$
We 1-4	1.46±0.07	≤ 10	61.8±6.18	12400 $^{+700}_{-600}$		

^a $R([\text{S II}]) = [\text{S II}] 6717/6731$; $R([\text{N II}]) = [\text{N II}] (6548+6584)/5755$.

^b $R([\text{O III}]) = [\text{O III}] (4959+5007)/4363$.

abundance (Kingdon & Ferland 1995). All other ion concentrations were computed with the *nebular* package. The determination of ion abundances is highly dependent on the temperature, but given the large volume of data no attempt was made to estimate errors from the temperature ranges given in Table 3. Following Bohigas (1998), ion concentrations were calculated with the following temperatures: O^0 , N^0 , N^+ , O^+ , and S^+ with $T(\text{N}^+)$; He^+ , S^{+2} , Ar^{+2} , and Cl^{+2} with $T(\text{N}^+)+[T(\text{O}^{+2})-T(\text{N}^+)]/3$; He^{+2} , O^{+2} , Ne^{+2} and Ar^{+3} with $T(\text{O}^{+2})$; and Ar^{+4} with $T(\text{O}^{+2})+1000$. In A 26, HDW 5, and We 1-4 it was not possible to determine the electron temperature from the oxygen lines and it was assumed that $T(\text{O}^{+2}) = T(\text{N}^+)+1000$ K.

Elemental abundances are also presented in Table 4. The helium abundance was determined from the He^+ concentration found from He I 5876, except for We 1-4, where He I 6678 was used since He I 5876 could not be measured confidently due to poor sky subtraction. Abundances from all the other elements were computed using the ionization correction factors given by Kingsburgh & Barlow (1994). When available, oxygen abundances were derived using the O^+ concentration from [O II] 3727. The oxygen abundance in A 26 and M 1-75 was found using [O II] 7320,7330. In We 1-4 there is no information

on the concentration of O^+ , and it is assumed that the oxygen abundance is equal to 2×10^{-4} .

3. DISCUSSION

3.1. General Properties

A summary of some of the properties of these objects is presented in Table 5. The logarithm of the total $\text{H}\alpha$ flux ($F\alpha$, not corrected for reddening) was derived from the flux calibrated $\text{H}\alpha$ images obtained for each object. The mass of ionized hydrogen can be determined from

$$M(\text{H}^+) = 4\pi D^2 I(\text{H}\beta) / \langle N_e \rangle E_{42} ,$$

where D is the distance to the object, $I(\text{H}\beta)$ is the reddening-corrected total $\text{H}\beta$ flux, $\langle N_e \rangle$ is the mean electron density and E_{42} is the effective recombination emissivity. Given the large uncertainty of the distances (Zhang 1995) and the mean electron density, the values of $M(\text{H}^+)$ given in Table 5 (in solar mass units) are for $D = 1$ kpc and $\langle N_e \rangle = 1 \text{ cm}^{-3}$. Errors were determined assuming that the nitrogen temperature ($T(\text{N}^+)$, used to calculate E_{42}) and $I(\text{H}\beta)$ are uncertain at the 10% level, and the extinction constant ($C(\text{H}\beta)$ from Table 2, used to find the reddening-corrected total $\text{H}\beta$ flux) can vary up to 30%. These large errors are largely due to

TABLE 4
ABUNDANCES

Ion	Line	A 26 ^a	BV 5-1	HDW 5 ^b	JnEr 1	K 3-72	K 3-92	K 3-94	K 4-55
He ⁺	5876	0.149	0.112	0.094	0.139	0.127	0.113	0.113	0.109
He ⁺²	4686		0.073		0.026	0.030	0.008	0.040	0.064
O ⁰ × 10 ⁻⁵	6300		4.13	3.26	5.53	3.87	3.85	8.09	2.37
O ⁺ × 10 ⁻⁴	3727		0.74	2.58	3.26	0.82	1.56	0.66	0.43
O ⁺ × 10 ⁻⁴	7325	1.16	1.04					0.79	0.51
O ⁺² × 10 ⁻⁴	5007	0.95	0.67	0.06	2.10	1.24	2.08	0.83	0.69
N ⁰ × 10 ⁻⁵	5200		1.09	0.24	0.33	2.81	0.15	0.39	0.64
N ⁺ × 10 ⁻⁵	6584	3.24	13.3	2.76	12.7	42.5	3.55	5.59	14.9
S ⁺ × 10 ⁻⁶	6717	0.71	3.00	2.18	0.66	1.85	0.94	1.14	1.85
S ⁺² × 10 ⁻⁶	6312		4.85			5.01		2.11	6.28
Ne ⁺² × 10 ⁻⁵	3869		2.94		10.3	7.56	7.10	2.63	2.75
Ar ⁺² × 10 ⁻⁶	7136	0.98	1.89		2.47			0.93	1.37
Ar ⁺³ × 10 ⁻⁷	4740		2.15						5.28
Ar ⁺⁴ × 10 ⁻⁷	6435,7006		0.94					1.88	
Cl ⁺² × 10 ⁻⁷	5528		1.06						
Element		A 26	BV 5-1	HDW 5	JnEr 1	K 3-72	K 3-92	K 3-94	K 4-55
He		0.149	0.185	0.094	0.165	0.157	0.121	0.153	0.173
O × 10 ⁻⁴		2.11	1.97	2.64	6.00	2.38	3.81	1.83	1.52
N × 10 ⁻⁴		0.59	3.54	0.28	2.33	12.3	0.87	1.55	5.27
S × 10 ⁻⁶		4.83	8.61	12.8	4.42	7.65	6.91	3.60	9.48
Ne × 10 ⁻⁵			8.64		29.4	14.5	13.0	5.78	6.06
Ar × 10 ⁻⁶		1.83	3.52		4.62			1.75	2.65

^a A 26 ion concentrations assuming that $T(\text{O}^{+2}) = 13,600$ K.

^b HDW 5 ion concentrations assuming that $T(\text{O}^{+2}) = 11,800$ K.

the generous allowance made on variations in the extinction constant. It should be pointed out that the H β images obtained in this work were not deep enough to produce extensive extinction maps when combined with the H α images.

Kaler & Jacoby (1989) provide simple formulae to estimate the effective temperature and visual magnitude (not corrected for reddening) of central stars in optically thick PNe. The temperature is determined from the relative intensity of He II 4686 with respect to H β (corrected for reddening). The determination of visual magnitudes also requires the observed H β (or H α) flux and the extinction constant $C(\text{H}\beta)$. They argue that a PN can be regarded as optically thick if $[\text{O II}] 3727/\text{H}\beta \geq 1$ (corrected for reddening). In this sample, objects with measurable He II 4686 fulfill this criterion. The temperature and visual magnitude of their central stars are given in Table 5 under the columns labelled T_c and

V_o . Notice that the spectral data from two regions in Sh 2-71 lead to conflicting results regarding the temperature: a substantially larger central star temperature is found in the region where $[\text{O II}] 3727$ is smaller (Sh 2-71 E). This suggests that it may be wiser to use a higher lower limit for the criterion defining an object as optically thick. If so, the central star temperatures derived for K 3-72 and K 4-55 should be regarded as upper limits. The same can be said for We 1-4, where no O⁺ line was measured. Errors in the visual magnitudes take into account the estimated precision of the spectral data used to calibrate the H α images and a 30% variation in the value of $C(\text{H}\beta)$ reported in Table 2. In this sample, there is only one direct determination of the visual magnitude of the central star: according to Liebert et al. (1988) the visual magnitude of the central star of JnEr 1 is 16.83, half a magnitude brighter than the value given in Table 5.

TABLE 4 (CONTINUED)

Ion	Line	M 1-41	M 1-75	M 2-52	M 2-53	Sh 2-71	E Sh 2-71	NE	We 1-4 ^{c,d}
He ⁺	5876	0.084	0.067	0.078	0.095	0.112	0.137		0.134
He ⁺²	4686	0.058	0.113	0.069	0.022	0.099	0.062		0.039
O ⁰ × 10 ⁻⁵	6300	3.21	4.65	1.45	5.08	2.84	2.29		3.06
O ⁺ × 10 ⁻⁴	3727	0.56		0.58	1.69	0.46	1.00		
O ⁺ × 10 ⁻⁴	7325	0.80	0.96			1.63			
O ⁺² × 10 ⁻⁴	5007	0.46	2.03	1.16	1.86	0.60	0.75		0.40
N ⁰ × 10 ⁻⁵	5200	0.93	1.48	0.43	0.45	1.07	0.63		0.59
N ⁺ × 10 ⁻⁵	6584	10.2	21.7	10.6	7.15	21.2	30.3		14.3
S ⁺ × 10 ⁻⁶	6717	1.92	3.13	1.70	1.44	3.51	4.05		0.95
S ⁺² × 10 ⁻⁶	6312	4.37	9.02	5.42	2.24	7.05	8.06		
Ne ⁺² × 10 ⁻⁵	3869	1.82	6.91	4.42	6.62	2.48	4.39		
Ar ⁺² × 10 ⁻⁶	7136	2.46	2.31			2.63	2.06		
Ar ⁺³ × 10 ⁻⁷	4740	3.65	11.0	2.68		4.60			
Ar ⁺⁴ × 10 ⁻⁷	6435,7006	2.62	0.85	1.05		1.07			
Cl ⁺² × 10 ⁻⁷	5528		3.25	1.08	1.01				
Element		M 1-41	M 1-75	M 2-52	M 2-53	Sh 2-71	E Sh 2-71	NE	We 1-4 ^e
He		0.142	0.180	0.147	0.117	0.211	0.199		0.173
O × 10 ⁻⁴		1.45	5.77	2.65	4.08	1.62	2.24		2.00
N × 10 ⁻⁴		2.64	13.1	4.84	1.73	7.47	6.79		2.22
S × 10 ⁻⁶		6.87	16.3	8.84	3.97	12.3	12.9		6.06
Ne × 10 ⁻⁵		5.74	19.6	10.1	14.5	6.70	13.1		
Ar × 10 ⁻⁶		5.03	4.19	0.61		4.46	3.85		

^c We 1-4 He⁺ concentration from He I 6678.

^dWe 1-4 ion concentrations assuming that $T(\text{O}^{+2}) = 13,400$ K.

^e We 1-4 abundances assuming that the oxygen abundance is 2×10^{-4} .

3.2. Individual Objects

a) A 26

The absence of He II 4686 in the spectrum of A 26 (Table 2) indicates that low levels of excitation prevail in this object. Not surprisingly, using the energy balance approach Preite-Martínez et al. (1991) found that the temperature of the central star is 68,000 K, much less than that of any other object in this sample. Lines from neutral ions (e.g., [N I] 5200 and [O I] 6300) are also absent in the spectrum, which implies that the nebula is optically thin. Since [O III] 4363 was not measured, it is assumed that $T(\text{O}^{+2}) = T(\text{N}^{+}) + 1000$ K. The helium abundance is ≥ 0.125 (Table 4) for any reasonable but large temperature range (from 10,000 to 14,000 K). On the other hand, the nitrogen-to-oxygen abundance ratio is 0.28. This combination ($\text{He}/\text{H} \geq 0.125$ and $\text{N}/\text{O} < 0.5$) has been observed

in other PNe (Kingsburg & Barlow 1994). Thus, A 26 can be classified as a non-type I PN with a high He abundance.

Images of A 26 in [N II] 6584, [N II] 6584/ $H\alpha$, $H2$, and [O III] 5007 are shown in Figure 1. Since the object was not detected through the cK filter, it follows that there is no major contribution from the continuum in the $H2$ frame. As can be seen, there is no hint of a bipolar morphology in any of these images, and the emitting gas revealed by the $H2$ frame is distributed over the entire nebula in structures that closely follow the distribution of [N II] 6584, with no evidence of a dense equatorial toroid. In consequence, it is likely that emission from He I at $2.11 \mu\text{m}$ is dominating the $H2$ image. Notice too that the absence of lines from neutral species in the optical spectrum and the conclusion derived from this, i.e., that the nebula is optically thin, argues against the existence of a large quantity of molecular hydro-

TABLE 5
GENERAL PROPERTIES

Object	Type	Mor.	He	N/O	N+O	HeR ^a	TR ^b	HS ^c	$-F\alpha$ ^d	M(H ⁺) ^e	T_c ^f	V_o ^g
A 26	I	E	0.149	0.28	2.70	0		5.26	11.91	4.61 ^{+7.61} _{-2.91}	.	.
BV 5-1	I	B	0.185	1.80	5.51	0.65	1.48	1.55	11.22	8.16 ^{+7.49} _{-3.99}	219.21.1	^{+0.2} _{-0.2}
HDW 5	IIb	B	0.094	0.11	2.92	0		2.52	10.71	21.9 ^{+19.0} _{-10.4}	.	.
JnEr 1	I	E,B?	0.165	0.39	8.33	0.17	1.08	8.51	10.35	18.6 ^{+7.19} _{-5.45}	129.17.4	^{+0.1} _{-0.1}
K 3-72	I	B	0.157	5.17	14.7	0.29	1.10	4.30	11.72	3.00 ^{+3.59} _{-1.66}	136.21.4	^{+0.3} _{-0.3}
K 3-92	IIb	Ea	0.121	0.23	4.68	0.13	1.34	5.34	12.07	2.60 ^{+4.07} _{-1.60}	94.21.5	^{+0.3} _{-0.3}
K 3-94	I	B	0.153	0.85	3.38	0.24	1.30	3.54	12.99	0.09 ^{+0.06} _{-0.04}	157.24.7	^{+0.2} _{-0.2}
K 4-55	I	B	0.173	3.47	6.79	0.59	1.38	2.67	11.89	5.85 ^{+11.1} _{-3.87}	201.23.0	^{+0.4} _{-0.4}
M 1-41	I	B	0.142	1.82	4.09	0.69	1.37	2.59	10.76	154 ⁺¹²⁸ ₋₁₁₁	190.20.2	^{+0.4} _{-0.4}
M 1-75	I	B	0.180	2.27	18.9	1.69	1.35	2.24	11.65	35.7 ⁺¹²⁸ _{-28.1}	358.23.9	^{+0.5} _{-0.5}
M 2-52	I	B	0.147	1.83	7.49	0.88	1.21	2.67	12.02	3.42 ^{+5.50} _{-2.13}	210.23.3	^{+0.3} _{-0.3}
M 2-53	IIa	Ea	0.117	0.42	5.81	0.23	1.17	4.84	11.21	6.02 ^{+4.98} _{-2.79}	122.19.7	^{+0.2} _{-0.2}
Sh 2-71 E	I	B	0.211	4.61	9.09	0.88	1.54	1.47	10.93	12.5 ^{+10.1} _{-5.72}	296.21.0	^{+0.2} _{-0.2}
Sh 2-71 NE	I	B	0.199	3.03	9.03	0.45	1.38	1.22	10.93	14.6 ^{+13.1} _{-7.06}	197.20.2	^{+0.2} _{-0.2}
We 1-4	I	B	0.173	1.11	4.22	0.29		4.18	12.05	1.46 ^{+1.48} _{-0.75}	154.22.5	^{+0.3} _{-0.3}

^aHeR = He⁺²/He⁺. ^bTR = $T(O^{+2})/T(N^{+})$.

^cHS = H α /[S II] 6724. ^d $F\alpha$ = logarithm of the total H α flux (not de-reddened).

^eM(H⁺) = mass of ionized hydrogen in solar mass units, for a distance of 1 kpc and $\langle N_e \rangle = 1 \text{ cm}^{-3}$.

^f T_c = central star temperature in 1000 K.

^g V_o = visual magnitude of the central star.

gen in this nebula. To sum up, A 26 is a faint low excitation elliptical non-type I PN with very little (if any) molecular hydrogen within it.

b) BV 5-1

BV 5-1 is characterized by high temperatures (Table 3), large intensity of He II 4686 (leading to He⁺²/He⁺ = 0.65), and a large helium abundance and nitrogen-to-oxygen abundance ratio (Table 4), both typical of type I PNe. It also stands out for the presence of lines from high and low ionization species with intensities comparable to the hydrogen Balmer lines and among themselves, which indicates that excitation conditions are very stratified along the line of sight. The high intensity of lines from low ionization species indicates that the nebula is at least partially optically thick (Kaler, Chu, & Jacoby 1988). The global nature of the spectrum (Table 2) also suggests that shock waves may have an effect on the plasma. Notice that H α /[S II] 6724 = 1.55 in BV 5-1, a value commonly observed in shock-excited

plasmas but substantially less than that of a typical photoionized nebula, where it is rarely smaller than ~ 2 . Consider too that $T(O^{+2})$ and $T(N^{+})$ are both very large (Table 3) and quite different ($T(O^{+2})/T(N^{+}) = 1.48$), a combination that is normally found in shock waves. This possibility casts some doubt on the accuracy of the abundance determinations. Finally, the effective temperature of the central star leads to a ZAMS progenitor with a mass of at least $\sim 3.5 M_{\odot}$ (Vassiliadis & Wood 1994; Blöcker 1995).

Images of BV 5-1 in [N II] 6584, [N II] 6584/H α , [O III] 5007/H α (not corrected for reddening), and $H2$ are displayed in Figure 2. The object was absent in the cK image. The most salient feature in the optical images is the extended bipolar structure opening to the SE, visible only in [N II] 6584, and extending some 4' away from the bright central disk, where the pincers of the lobe appear to close on each other. Faint traces of the NW counterpart of the bipole can also be found in this image.

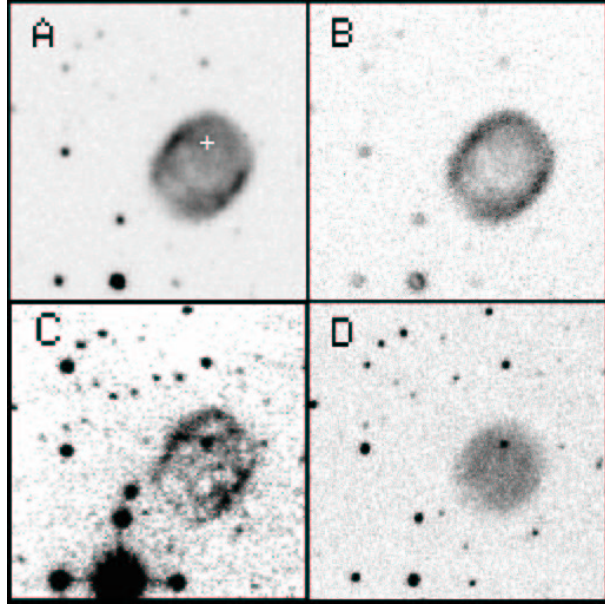


Fig. 1. A 26: (A) [N II] 6584, (B) [N II] 6584/H α , (C) H 2 , and (D) [O III] 5007. The position where the spectrum was taken is marked by a cross in (A). The field of view (FOV) is $110'' \times 110''$. North is up, east is to the left.

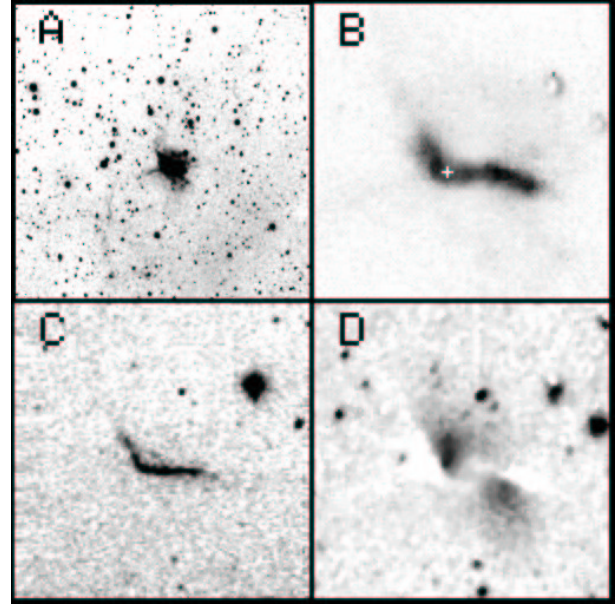


Fig. 2. BV 5-1: (A) [N II] 6584, (B) [N II] 6584/H α , (C) H 2 , and (D) [O III] 5007/H α (not corrected for reddening and with a 3×3 median filter applied). A cross in (B) marks the position where the spectrum was taken. The FOV is $620'' \times 620''$ in (A) and $110'' \times 110''$ in the other three frames. North is up, east is to the left.

This extended structure clearly demonstrates that BV 5-1 is a bipolar PN, as was classified in the IAC-Catalog. The [O III] 5007/H α image, which has not been corrected for reddening, displays a slanted distribution. From an H β image it was possible to apply an extinction correction to the brightest region of BV 5-1, and it was found that the distribution of [O III] 5007/H α is mainly due to changes in the excitation conditions, though a central dust lane where $C(H\beta)$ is roughly constant, originally found by Kaler et al. (1988), does soften the contrast. Notice that this S-like pattern is replicated in the other images, and it suggests that a structure close to the central star may induce this asymmetric morphology. In relation to this it is worth noticing that Josselin et al. (2000) found that the molecular gas, as evinced by CO observations, forms an irregular ring which appears to be perpendicular to the bipolar nebula. An additional feature of the optical images is that faint extended H α emission (the image is not shown) surrounds BV 5-1, but it does not appear to be associated to this PN. The bipolar morphology, the absence of emission in the cK image, and the existence of a toroid in the H 2 frame strongly support the hypothesis that shock-excited H 2 emission is present in BV 5-1.

c) HDW 5

Based on the low intensity of the [O III] lines and its very peculiar morphology, Ali & Pfeiderer (1999) doubt on the identity of HDW 5 as a PN. The spectrum presented here (Table 2) is almost identical to the one obtained by Ali & Pfeiderer (1999), with the important addition of a measured flux for [O II] 3727. Since [O III] 4363 could not be measured, ion abundances were calculated assuming that $T(O^{+2}) = T(N^+) + 1000$ K. If HDW 5 is a PN, the chemical composition (Table 4) of this very low excitation object implies that it can be classified as type IIb (Faúndez-Abans & Maciel 1987). But notice that the helium abundance and the sum of the oxygen and nitrogen abundances are as low as in typical galactic H II regions. On the other hand, $H\alpha/[S II] 6724 = 2.52$, which is rather small for an H II region.

Images of HDW 5 are displayed in Figure 3. Since no image was taken through the cK filter, the frame labelled as H 2 cannot be regarded as representative of line emission. Even so, the morphology of the region revealed by this image, with a central bar and the eastern extensions emerging from it, suggests the

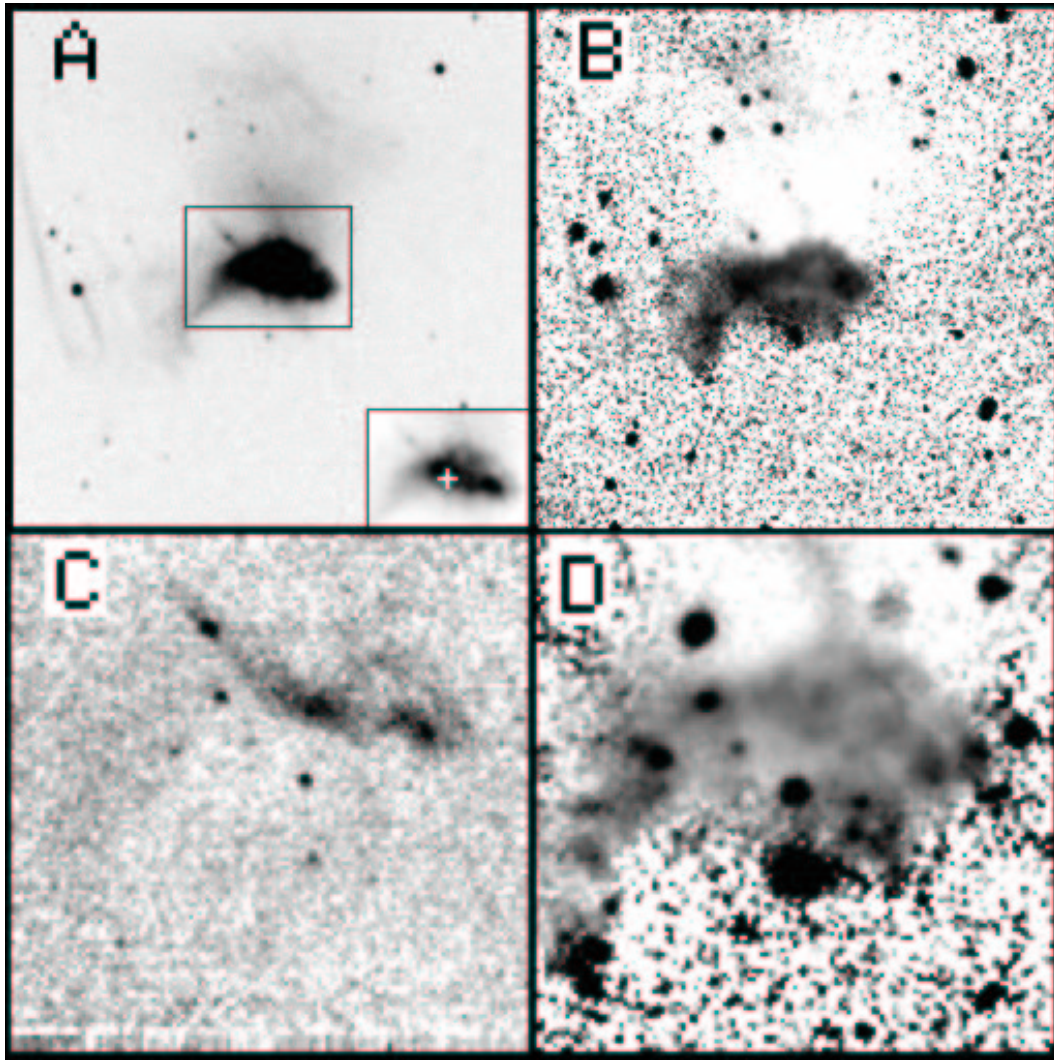


Fig. 3. HDW 5 : (A) $H\alpha$, (B) $[\text{N II}] 6584/H\alpha$, (C) H_2 , and (D) $[\text{S II}] 6724/H\alpha$. The central region of the $H\alpha$ image is displayed in the (A) subframe, where the position where the spectrum was taken is marked with a cross. The FOV is $256'' \times 256''$ in (A) and (B), $110'' \times 110''$ in (C) and (D). North is up, east is to the left.

existence of shocked molecular hydrogen. This is puzzling given the spectral properties of HDW 5. Images of this object in $H\alpha$ (with the central region displayed in a sub-frame), $[\text{N II}] 6584/H\alpha$ and $[\text{S II}] 6724/H\alpha$ are also presented in Fig. 3. The line ratio images show a large contrast between the extended fan opening to the north of the central bar and the latter, where $[\text{N II}] 6584$ and $[\text{S II}] 6724$ emission is concentrated. Low excitation condensations distributed over the whole extent of the central bar are evident in the $[\text{S II}] 6724/H\alpha$ frame. Notice that the regions where the H_2 image is brighter are those where $[\text{S II}] 6724/H\alpha$ and $[\text{N II}] 6584/H\alpha$ are larger. Were it not for the prominent $H\alpha$ filaments

seen to the east of the brightest region, these images would suggest that HDW 5 is a bipolar PN with a very bright central ring confining the outflow, as advanced in the IAC-Catalog. But Ali & Pfeiderer (1999) emphatically argue that this cannot be so, since the possible exciting star (Méndez 1991) is detached from the main body of HDW 5, though this candidacy is still to be confirmed. Also, if HDW 5 is a PN, its chemical composition seems to be at odds with a bipolar morphology, i.e., type I Ib PNe are not usually bipolar. Needless to say, additional work is required. Research on the nature of the IR emission revealed in the H_2 image may suffice to establish the true nature of this object.

d) JnEr 1

This PN is one of the few with a PG 1159 type central star (Liebert et al. 1988). Spectroscopy of this large nebula was performed with the slit centered on the NW region (see Figure 5). The oxygen and neon abundances (Table 4) are the largest in the sample, but both are probably correct (if the ionization correction factors are adequate) since [O II] 3727 and [Ne III] 3869 are very intense. The large helium abundance (0.165) is typical of a type I PN, but the nitrogen-to-oxygen abundance ratio (0.39) suggests otherwise. The reported N/O ratio is considerably less than the value derived by Kaler (1983b) from large aperture photometric observations (his entry name for the nebula is NGC 2474-5). Based on a much lower intensity for [O II] 3727 (258 versus 806) he finds that $N/O = 1.2$. Since the combination of large helium, oxygen and neon abundances with a relatively small N/O ratio is difficult to grasp (a third dredge-up without nitrogen enrichment), these data may imply that JnEr 1 is not chemically homogeneous, and that the region observed in this work is abnormally abundant in oxygen. Given its chemical composition, size and central star temperature, JnEr 1 can be tentatively classified as an evolved, moderately excited (low temperatures, see Table 3, and $He^{+2}/He^+ = 0.19$) type I PN produced by a $\sim 3.0 M_{\odot}$ ZAMS progenitor (Vassiliadis & Wood 1994).

Images of JnEr 1 in [N II] 6584, [O III] 5007, [N II] 6584/H α and [O III] 5007/H α (not corrected for reddening) are displayed in Figure 4. H α and [O III] 5007 images for the entire object were not obtained. Not surprisingly, from the morphological point of view JnEr 1 has been classified as an elliptical PN (IAC-Catalog). But a couple of features lead to suspect that it may be a bipolar seen almost pole-on: the faint outer filamentary arch at the NE may be the lobe lying on the far side (it can be argued that it is an external envelope, as in IC 1295, but in this case it is not symmetric) and the brightest regions may be defining the evolved expanded disk confining the outflow. The chemical composition gives some support to this possibility. Given the size of this object, infrared observations were only carried out in the two brightest optical fields (Fig. 5). Nothing was detected through the *cK* filter, so that it can be concluded that the features observed in the *H2* frames are not due to continuum emission. The *H2* image may be dominated by He I line emission at $2.11 \mu m$ since it is not evident that there is an equatorial density enhancement. This hypothesis is agreeable to the possible classification of

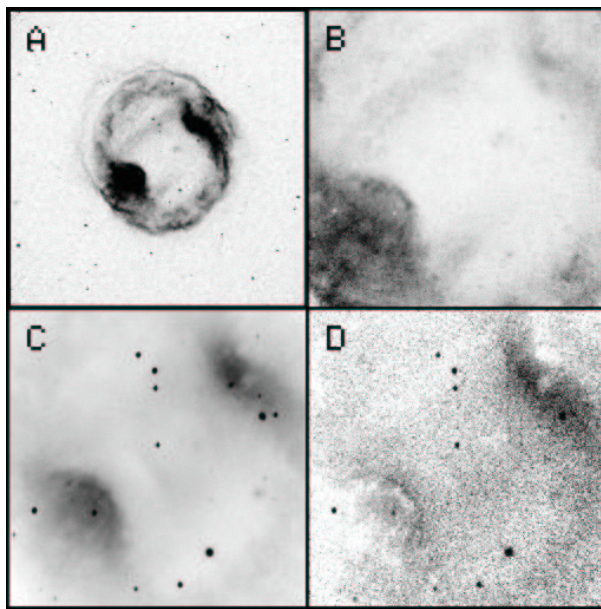


Fig. 4. JnEr 1 : (A) [N II] 6584, (B) [N II] 6584/H α , (C) [O III] 5007 and (D) [O III] 5007/H α (not corrected for reddening). The FOV is $620'' \times 620''$ in (A). In the other frames, it is $256'' \times 256''$. North is up, east is to the left.

JnEr 1 as an elliptical PN. But notice that the existence of shock-excited H $_2$ emission cannot be entirely discarded since Huggins et al. (1996) discovered CO emission in this object (though the derived molecular mass is only $0.0028 M_{\odot}$, or 0.017 times the mass of ionized gas).

e) K 3-72

The most outstanding feature in the spectrum of K 3-72 (Table 2) is the exceptionally high intensity of the N $^+$ lines ([N II] 6584/H $\alpha = 6.34$), surpassed only in the NE region of Sh 2-71. Not surprisingly, nitrogen is notoriously overabundant (Table 4), which leads to one of the highest N/O ratios ever reported in a planetary nebula (5.17). Helium is also overabundant (0.157), though not exceptionally so. The excitation conditions of this type I PN are relatively mild (at least in the observed region), judging from the intensity of [O III] 5007, the low temperatures (Table 3), and the comparatively small He^{+2}/He^+ ratio (0.24) with respect to other type I PNe in the sample. Notice too that both $T(O^{+2})/T(N^+) = 1.10$ and $H\alpha/[S II] 6724 = 4.30$ indicate that shocks have a minor importance in the inspected region. This implies that the very large [N II] 6584/H α ratio does not result from shock excitation, and that the abundance of nitrogen with respect to oxygen may be real. It is exceedingly dif-

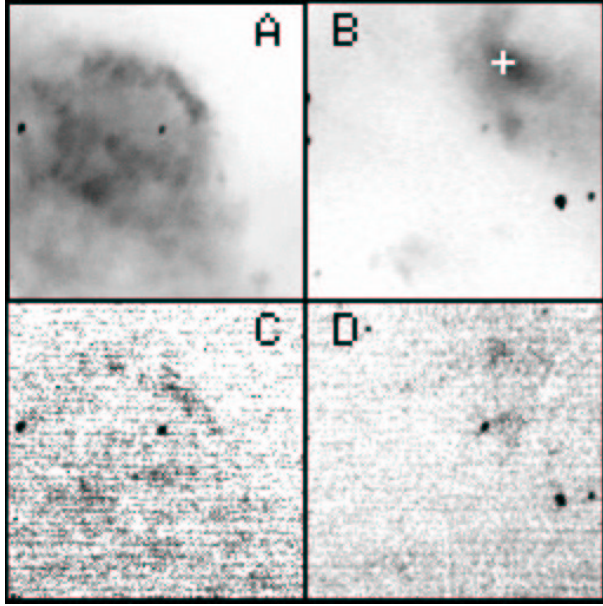


Fig. 5. JnEr 1 : SE region in (A) [N II] 6584 and (C) H_2 , NW region in (B) [N II] 6584 and (D) H_2 . The position where the spectrum was taken is marked by a cross in (B). The FOV is $110'' \times 110''$. North is up, east is to the left.

difficult to explain this ratio with current models of stellar evolution. A large production of nitrogen in an envelope burning primary carbon brought to the surface by a third dredge-up (see Iben 1995) would be required. This can be achieved if the PNN is massive enough, i.e., has a large ZAMS progenitor mass. The large values for the abundance of neon and the sum of the nitrogen and oxygen abundances are consistent with this hypothesis. But the central star temperature (see Table 5) indicates that the progenitor mass is $\leq 3.5 M_{\odot}$ (Vassiliadis & Wood 1994; Blöcker 1995). Furthermore, the central star temperature annotated in Table 5 may be too large (consequently also the mass of the PNN) since it is possible that the observed region is not optically thick (see § 3.1).

Images of K 3–72 in [N II] 6584 (logarithmic scale), [N II] 6584/ $H\alpha$, [O III] 5007/ $H\alpha$ (not corrected for reddening) and H_2 are displayed in Figure 6. The [N II] 6584 image is scaled in order to show the extended emission that defines a tight bipolar structure. The central $34'' \times 34''$ of the [N II] 6584 image, where the object is more than 100 times brighter than in the faint bipolar lobes, is shown in a sub-frame. The torus confining the outflow of material is evinced in this sub-frame by two bright spots defining a line perpendicular to the

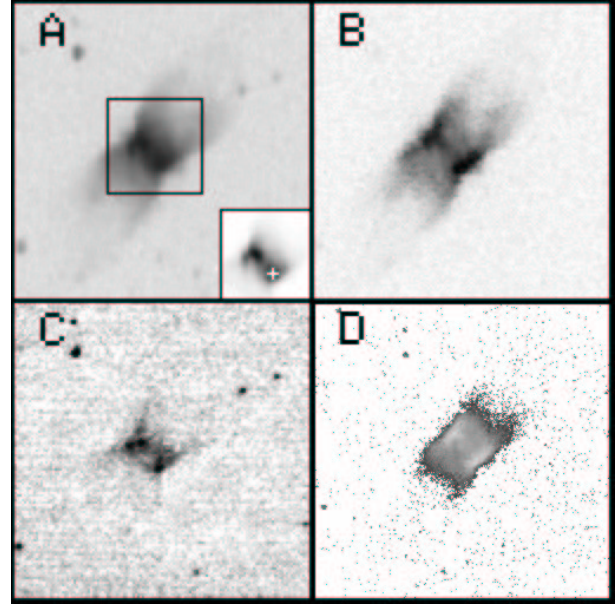


Fig. 6. K 3–72: (A) [N II] 6584 (logarithmic scale), (B) [N II] 6584/ $H\alpha$, (C) H_2 , and (D) [O III] 5007/ $H\alpha$ (corrected for reddening). The central region of the [N II] 6584 image is displayed in the (A) subframe, where the position where the spectrum was taken is marked with a cross. The FOV in the main frames is $110'' \times 110''$. North is up, east is to the left.

bipolar structure. These bright spots are also seen in $H\alpha$, [S II] 6724, and [O III] 5007 images (not shown). The presence of H_2 is inferred from the torus and the opening of the bipolar structure that are sharply delineated in the H_2 image. Extended emission was also detected in the cK frame, but it is so faint that there can be little doubt that molecular hydrogen emission is excited by shock waves. As expected, the diameter of the torus, defined by the separation of the two bright spots, increases as regions with lower excitation are considered: $\sim 12''$ in H_2 , $\sim 9''$ in [N II] 6584, and $\sim 6''$ in [O III] 5007. There is no hint of an inner structure in either image, so that it follows that the outflow is, in all probability, only confined by this torus.

f) K 3–92

Chemical abundances (Table 4) imply that K 3–92 is, according to Peimbert's (1990) criteria, either a type II or type III PN. The average height above the Galactic plane of type II PNe is 150 pc, which corresponds to progenitors of $\simeq 1.5 M_{\odot}$, whereas type III PNe are found at $|z| > 800$ pc and are the end product of population II stars. The distance to K 3–92 ranges from 15.58 kpc (Zhang 1995) to

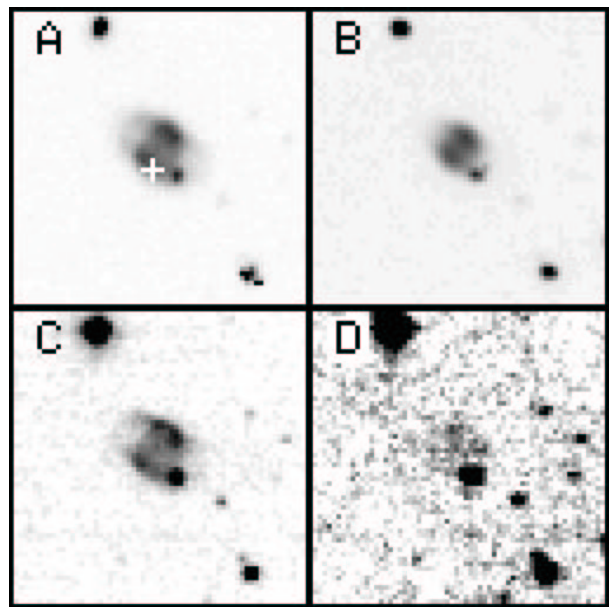


Fig. 7. K 3-92: (A) [N II] 6584, (B) [O III] 5007, (C) H_2 , and (D) cK . The position where the spectrum was taken is marked by a cross in (A). The FOV is $55'' \times 55''$. North is up, east is to the left.

6.81 kpc (Cahn, Kaler, & Stanghellini 1992), leading to $|z|$ between 400 and 800 pc. It follows that K 3-92 is quite probably a type II PN (more precisely, type IIb according to Faúndez-Abans & Maciel 1987).

Images of K 3-92 in [N II] 6584, [O III] 5007, H_2 , and cK are presented in Figure 7. An elliptical morphology (type Ea, following the IAC-Catalog) is evident in all frames. The spectrum and morphology of K 3-92 suggests that the bright emission seen in the H_2 frame may be produced by the He I lines at $2.11 \mu\text{m}$. But notice that the extension of K 3-92 is markedly different in the [O III] 5007 ($\sim 4''$), [N II] 6584 ($\sim 6''$) and H_2 ($\sim 8''$) frames. This size arrangement can be explained if the H_2 image is representative of molecular hydrogen emission. Faint diffuse emission is found in the cK frame. A quick inspection of the H_2/cK image ratio (matching the background and then the star counts) yields values of at least 9 to 10 even where the nebula is brightest in the cK image. Thus, unless densities in the molecular gas are in excess of 10^5 cm^{-3} (a huge contrast with the density in the optical region, 245 cm^{-3}), H_2 emission is probably excited by shock waves. The persistence of H_2 emission arising from the inner boundary of the molecular gas indicates that this type IIb PN is relatively young. From this and its central star temperature, it can be concluded that the ZAMS progenitor mass is around $2 M_\odot$.

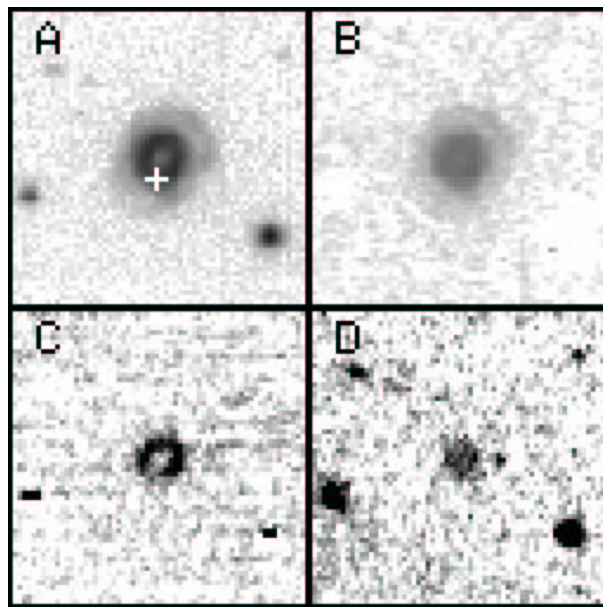


Fig. 8. K 3-94 in (A) [N II] 6584 (logarithmic scale), (B) $H\alpha/H\beta$, (C) $H_2 - cK$, and (D) cK . The position where the spectrum was taken is marked by a cross in (A). The FOV is $55'' \times 55''$. North is up, east is to the left.

g) K 3-94

K 3-94 is a mildly excited type I PN with no particularly interesting feature in its spectrum (Table 2). Images of this object in [N II] 6584 (logarithmic scale), $H\alpha/H\beta$, $H_2 - cK$, and cK are displayed in Figure 8. The optical nebular structure, consistent of a bright annulus surrounded by exceedingly faint arches pointing to the SE and NW, suggests that K 3-94 is a bipolar PN seen nearly pole-on, as catalogued in the IAC-Catalog. The $H\alpha/H\beta$ frame shows that extinction in the ring is substantially larger than in the faint arches ($C(H\beta) \sim 0.6$ versus 0.2), though it is quite uniform within both structures. The overall properties of K 3-94 indicate that shock excited H_2 emission is evinced in the H_2 image. It is concentrated in an annular structure that is slightly larger (6 versus $5''$) but thinner (2 versus $2.5''$) than that seen in the light of [N II] 6584. The faint patches observed to the west of the object in the $H_2 - cK$ frame are probably the residue of a stellar image. Faint and uniform emission from the central region is seen in the cK image. It is not induced by shock excitation, but it cannot be established if it is produced by dust or by fluorescent H_2 emission. It should be noticed that Josselin et al. (2000) detected (but did not resolve) CO emission from K 3-94, and determined that the molecular mass is approximately $0.034 M_\odot$ (~ 0.18 times the mass in ionized gas).

h) K 4–55

Optical imaging and high and low resolution spectroscopy of this type I PN was produced by Guerrero, Machado, & Serra-Ricart (1996), and more recently Guerrero et al. (2000) obtained H_2 and $Br\gamma$ images of the object. The spectrum presented in Table 2 is from a region in the southern edge of the bright inner ring, and should be compared with the averaged spectrum of region R reported by Guerrero et al. (1996), who assume that extinction is practically uniform. The $C(H\beta)$ image presented in Figure 9 clearly shows that this is not so; $C(H\beta)$ is obviously larger (but still not uniform) in the inner ring than in the surrounding gas, where it is $\simeq 1$. This may explain why the Balmer series line ratios given by these authors differ from the theoretical values. Similar forbidden line strengths are found here, but both temperatures are somewhat larger (Table 3) and lead to smaller concentrations for oxygen and nitrogen and a smaller N/O abundance ratio (Table 4). If the spectrum has not been substantially modified by shock waves, the large value for N/O (3.47) suggests that third dredge-up episodes occurred in K 4–55. The large central star temperature is also indicative of a massive progenitor.

Images of K 4–55 in $[N II] 6584$ (logarithmic scale), $[N II] 6584/H\alpha$, $C(H\beta)$, and H_2 are displayed in Fig. 9. The source was not seen through the cK filter. Based on kinematical arguments, Guerrero et al. (1996) conclude that this object is a bipolar PN seen nearly edge on. The configuration of the faint bipolar lobes seen in the $[N II] 6584$ frame vindicates their model. Their spectroscopic observations indicate that there is a faint extended halo visible in the Balmer lines and $[O III] 5007$, a result that could not be confirmed. The characteristics of K 4–55 imply that the emission seen through the H_2 image is due to shocked molecular hydrogen. Finally, images show with great clarity how the degree of excitation decreases away from the center: for instance, in the western side of the inner ring $[O III] 5007$ (not shown), $[N II] 6584$ and H_2 emission peak $\sim 5''$, $6.5''$, and $7.5''$ from the geometrical center.

i) M 1–41

From its IRAS spectrum and large radio flux density Zijlstra, Pottasch, & Bignell (1990) concluded that M 1–41 may be an H II region. This conclusion is probably incorrect: the spectral properties of M 1–41 and the presence of H_2 emission

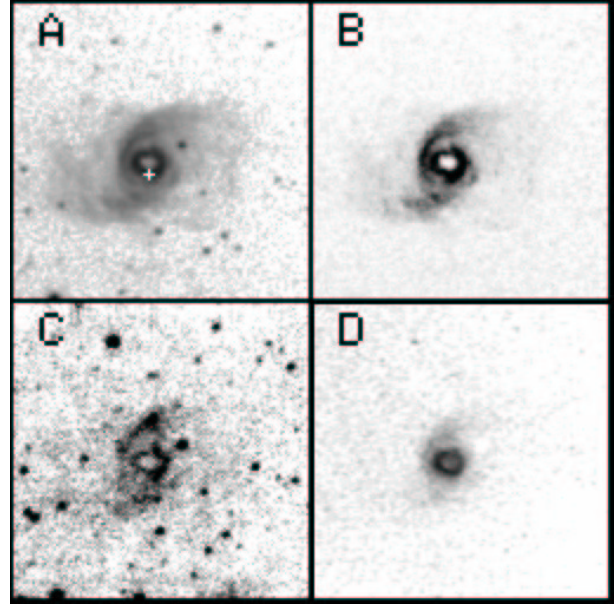


Fig. 9. K 4–55: (A) $[N II] 6584$ (logarithmic scale), (B) $[N II] 6584/H\alpha$, (C) H_2 , and (D) $C(H\beta)$. The position where the spectrum was taken is marked by a cross in (A). The FOV is $110'' \times 110''$. North is up, east is to the left.

within it (see below), indicate that it is a PN. The spectrum presented here (Table 2) is similar to the one reported by Dopita (1977), but very different from that obtained by Acker et al. (1991) regarding the $[N II] 6584/H\alpha$ line ratio (3.45 in this work versus 0.61 in Acker et al.). The high intensity of $He II 4686$ and the presence of $[Ar V]$ lines imply that M 1–41 cannot be an H II region. Furthermore, the spectral properties of M 1–41 are very similar to those found in other objects that have been unambiguously identified as PNe, such as BV 5–1 or Sh 2–71: extensive evidence of a very high degree of excitation (such as the presence of $[Ar V]$ lines or $He^{+2}/He^+ = 0.7$), strong lines from low ionization species (for instance, $H\alpha/[S II] 6724 = 2.59$ in M 1–41), very high temperatures (in this case the highest in the sample, see Table 3) and a large difference between the oxygen and nitrogen temperatures (in this case $T(O^{+2})/T(N^+) = 1.37$). As in those objects, the spectrum implies that the nebula is optically thick and/or shock waves are altering the spectral properties from what would be pure photoionization by the central star. These properties, and above all its chemical composition (Table 4), leave no doubt that M 1–41 is a type I PN. Finally, take notice that Preite-Martínez et al. (1991) derive a central star temperature of 142,400 K using the energy balance

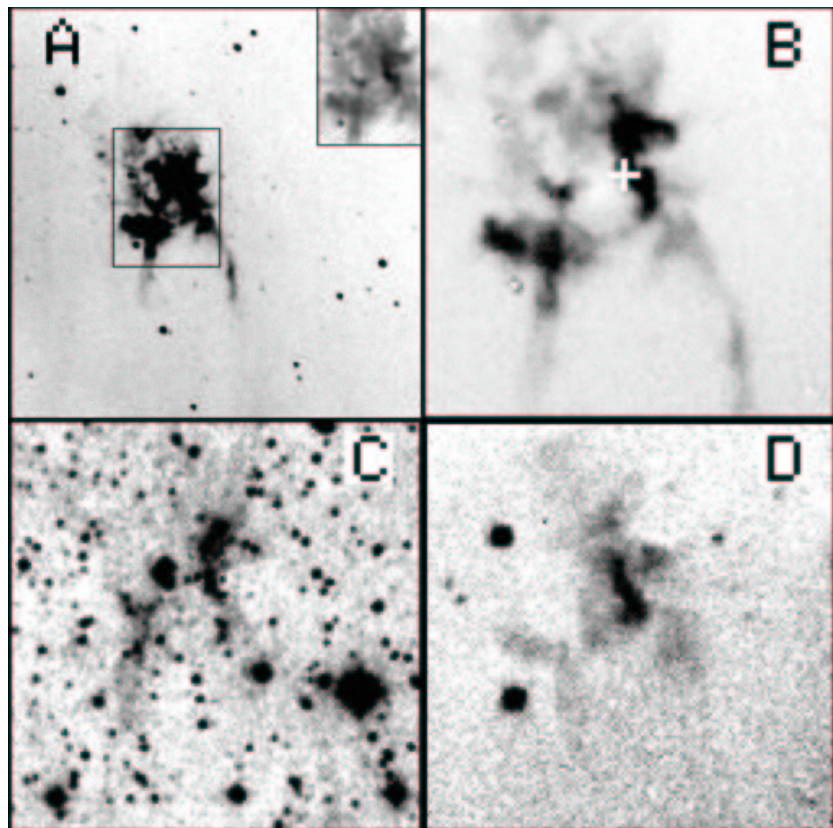


Fig. 10. M 1–41: (A) [N II] 6584 (logarithmic scale), (B) [N II] 6584/ $H\alpha$, (C) H_2 , and (D) [O III] 5007/ $H\alpha$ (not corrected for reddening). The central region of the [N II] 6584 image is displayed in the (A) subframe. The position where the spectrum was taken is marked by a cross in frame (B). The FOV is $256'' \times 256''$ in (A) and $110'' \times 110''$ in (B), (C), and (D). North is up, east is to the left.

approach, nearly 50,000 K less than the value reported in Table 5 following Kaler & Jacoby (1989).

Images of M 1–41 in [N II] 6584 (with a sub-frame showing the brightest region), [N II] 6584/ $H\alpha$, [O III] 5007/ $H\alpha$ (not corrected for reddening) and H_2 are presented in Figure 10. The overall morphology is similar in all images. The object is clearly bipolar, though the northern lobe is disrupted in a large number of chaotically distributed regions (most of them present in all frames). The inner boundary of the torus that confines the outflow, approximately aligned along an ESE – WNW axis, is well defined in the H_2 and [N II] 6584/ $H\alpha$ images. In the [N II] 6584/ $H\alpha$ image notice the structures that are disposed symmetrically with respect to the approximate center of M 1–41 (to the SE and NW). Finally, there is little doubt that there is extended shock excited H_2 emission within M 1–41. Its existence provides additional evidence that this object is a PN.

j) M 1–75

Aller & Keyes (1987) obtained an excellent spectrum of this object covering a large wavelength interval (from [Ne V] 3426 to [Ar III] 7751), but failed to detect [O III] 4363, and the temperature in the more highly excited regions could not be measured. Guerrero, Stanghellini, & Manchado (1995) measured this line adding two slit positions of spectroscopically similar regions in the inner ring (see Figure 11). Their extinction correction is doubtful since $H\gamma$ turns out too large. Furthermore, an $H\alpha/H\beta$ frame (not shown) proves that extinction is not uniform, contrary to that assumed by these authors. The spectrum presented here (Table 2) is from the eastern side of the inner ring, where extinction reaches its highest values, preventing the detection of the O^+ doublet at $\lambda 3727$. The Balmer series is satisfactorily reproduced up to $H\delta$. The most remarkable feature is the extreme strength of the He II 4686 Å line, which leads

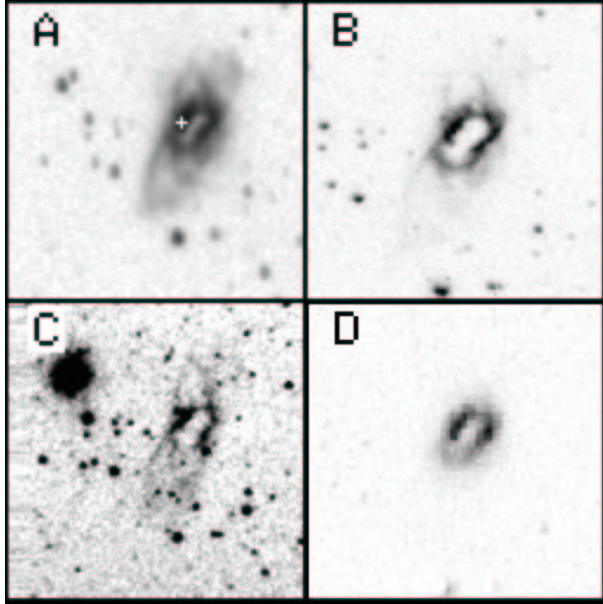


Fig. 11. M 1-75: (A) [N II] 6584 (logarithmic scale), (B) [N II] 6584/H α , (C) H 2 , and (D) [O III] 5007/H α (corrected for reddening). The position where the spectrum was taken is marked by a cross in (A). The FOV is 81'' \times 81'' in frames (B) and (D), 110'' \times 110'' in the other two. North is up, east is to the left.

to the highest He⁺²/He⁺ ratio (equal to 1.7) in the sample. Chemical abundances (Table 4) are more closely matched to those reported by Aller & Keyes (1987) than to those given by Guerrero et al. (1995), and have the unmistakable signature of a type I PN. As in other type I PNe, lines from low ionization species are intense, and there is a substantial difference between the oxygen and nitrogen temperatures ($T(\text{O}^{+2})/T(\text{N}^+) = 1.38$, see Table 3). The temperature of the PNN is very high (358,000 K), which means that it is quite massive. A ZAMS progenitor mass of at least 5 M_{\odot} can be deduced from post-AGB models (Vassiliadis & Wood 1994; Blöcker 1995). Notice that a massive progenitor can also be inferred from the chemical setup of M 1-75 (assuming that shock excitation is not prevalent), since it implies a third dredge-up. But massive PNN evolve very rapidly, and this large temperature occurs within the first hundred years or so of their lifetime. The images of M 1-75 suggest that this object cannot be so young. In consequence, either the effective temperature of the central star is smaller than the value reported in Table 5, or massive PNN do not evolve as fast as models predict.

Images of M 1-75 in [N II] 6584 (logarithmic scale), [N II] 6584/H α , [O III] 5007/H α (corrected

for reddening), and H 2 (almost certainly produced by H 2 line emission) are presented in Fig. 11. There is little to add to the excellent optical and infrared images produced by Guerrero et al. (1995, 2000), except for the non-detection of M 1-75 in the *cK* frame, which proves that H 2 is excited by shock waves, and the tight correlation between the [N II] 6584 and H 2 emitting regions.

k) M 2-52

The spectrum (Table 2) of this type I PN (He/H = 0.147 and N/O = 1.83, see Table 4) is characterized by a high degree of excitation (He⁺²/He⁺ = 0.9 and [Ar V] 6435 present), large temperatures (Table 3) and strong lines from low ionization stages (H α /[S II] 6724 = 2.67). The central star temperature implies a ZAMS progenitor with a mass of at least $\sim 3.5 M_{\odot}$ (Vassiliadis & Wood 1994; Blöcker 1995). Faint extended emission delineating a bipolar structure can be seen in an overexposed [N II] 6584 image (see Figure 12). The central region of this image, displayed in a subframe, shows the toroid that probably confines the outflow. It is also seen in the [N II] 6584/H α image, though it is rather diffuse, and certainly not as prominent as in other objects with similar spectral properties. An [O III] 5007/H α image (corrected for reddening) is also shown in Fig. 12. The ratio is quite uniform in the region confined by the torus, also in contrast with what is seen in other type I PNe, where [O III] 5007/H α is notoriously larger in the inner face of the torus. The H 2 image presented in Fig. 12 is underexposed. A much better image, where H 2 emission is seen to follow closely the distribution of [N II] 6584, was produced by Guerrero et al. (2000). No evidence of the PN was found in a *cK* image, which implies that H 2 emission is shock-excited. Finally, CO has been found in M 2-52 (Sun et al. 1998; Zhang, Sun, & Ping 2000), and a molecular mass of 0.085 M_{\odot} was inferred from these observations.

l) M 2-53

The chemical make-up of M 2-53 (Table 4) is characteristic of a type IIa planetary nebula (Faúndez-Abans & Maciel 1987), which implies a progenitor mass close to 2 M_{\odot} . The central star temperature is consistent with this estimate. No indication of a bipolar structure is to be seen in the [N II] 6584, [N II] 6584/H α , H 2 , and *cK* images presented in Figure 13. Following the IAC-Catalog, the object can be classified as type Ea from the morphological point of view. The properties of M 2-53 imply that the H 2 frame is dominated by emission from

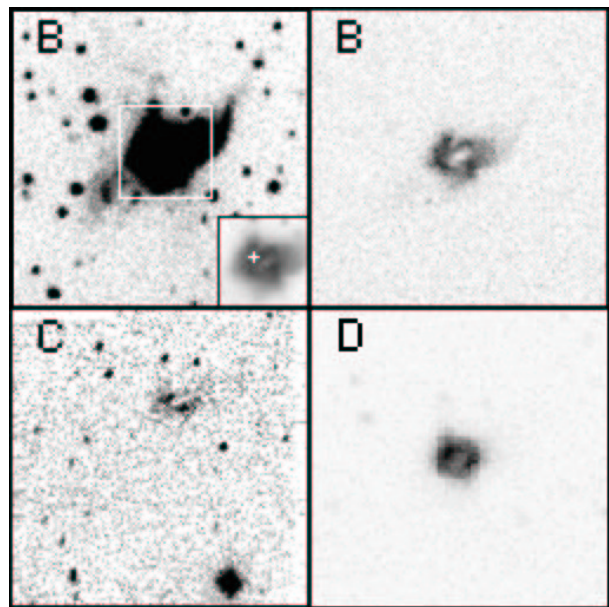


Fig. 12. M 2-52: (A) [N II] 6584 (logarithmic scale), (B) [N II] 6584/H α , (C) H 2 , and (D) [O III] 5007/H α (corrected for redening). The central region of the [N II] 6584 image is displayed in the (A) subframe, where the position where the spectrum was taken is marked with a cross. The FOV is $110'' \times 110''$ in frames (A), (B), and (C), and $81'' \times 81''$ in frame (D). North is up, east is to the left.

He I at $2.11 \mu\text{m}$. This is supported by these images, since the extension of the source in the H 2 image is obviously smaller than in the light of [N II] 6584. An unexpected (and unexplained) structure in the *cK* frame is seen to the south of M 2-53 (enclosed in a box). It cannot be a continuum emission source since it is not observed in the H 2 image, but it does not seem to be an observational artifact.

m) Sh 2-71

Kohoutek (1979) found that the PNN of Sh 2-71 is actually a binary, and concluded that the primary is a B8 type star, with an unseen companion with a temperature of at least 60,000 K (Glushkov, Denisyuk & Karyagina 1975). High resolution spectroscopy of the central region of Sh 2-71 (Cuesta & Phillips 1993) revealed a core with velocities $\pm 500 \text{ km s}^{-1}$ surrounded by an expanding $\sim 100''$ disc. These and other data led Cuesta & Phillips (1993) to propose that the kinematics are due to accretion from a late A or early F type main sequence star onto a companion with a temperature of 77,000 K (Kaler 1983b).

Previous spectroscopic observations had established that this is a type I PN (Sabbadin, Falomo,

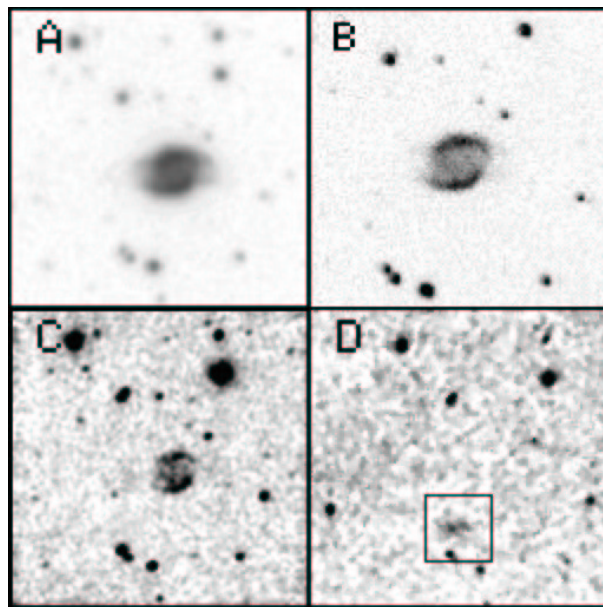


Fig. 13. M 2-53: (A) [N II] 6584 (logarithmic scale), (B) [N II] 6584/H α , (C) H 2 , and (D) *cK*. The position where the spectrum was taken is marked by a cross in (A). The FOV is $110'' \times 110''$ in (A), (C), and (D), and $81'' \times 81''$ in (B). Notice the small nebulosity in the *cK* frame (enclosed in a box). North is up, east is to the left.

& Ortolani 1987), but no additional conclusions could be advanced since information was rather limited. The spectra presented here (Table 2) are from two regions in the outer envelope. Region E, which is closer to the central star, is clearly more highly excited judging from the He $^{+2}$ /He $^{+}$ ratio (0.9 versus 0.5), the presence of the [Ar V] 7006 line and the oxygen temperature (17,600 versus 15,700 K, see Table 3). As in other type I PNe, Balmer and forbidden line intensities are comparable, lines from low and high ionization states can have similar intensities, and there is a large difference between the oxygen and nitrogen temperatures ($T(\text{O}^{+2})/T(\text{N}^{+}) = 1.54$ and 1.38 in regions E and NE, respectively), the former being quite high. If it is also taken into consideration that H α /[S II] 6724 is equal to 1.46 in region E and 1.22 in region NE, it can be asserted that Sh 2-71 is a good example of a PN where shock waves probably have a substantial effect on the emission spectrum, and this may be related to the high velocity outflow discovered by Cuesta & Phillips (1993). It is then likely that both spectra are affected by shock wave excitation, so that at least some the abundances determined here (Table 4) may be uncertain. Nearly the same large helium abundance (He/H $\simeq 0.2$) is

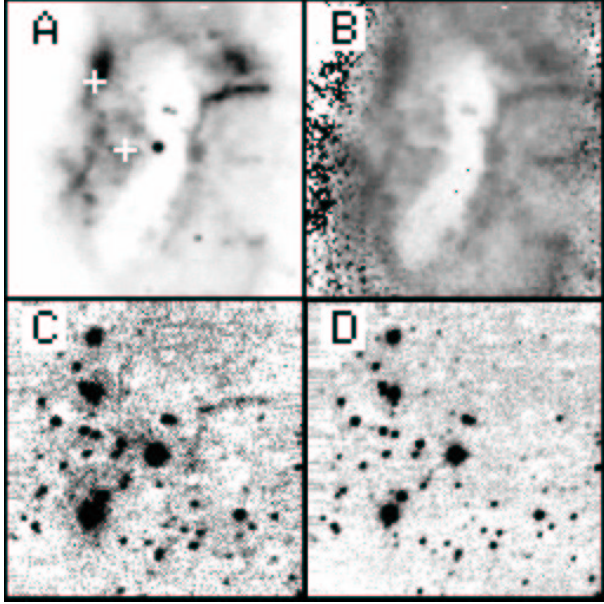


Fig. 14. Sh 2-71: (A) [N II] 6584, (B) [N II] 6584/H α , (C) H 2 , and cK . Positions where the spectra were taken are marked with crosses in (A). The FOV is 110'' \times 110''. North is up, east is to the left.

obtained in both regions, and similar values are found for the concentrations of nitrogen, sulfur and argon. But significant differences are found for oxygen and neon in particular. The N/O ratio is between 3.0 (region NE) and 4.6 (region E). The large (but questionable) values for the sum of the N and O abundances, and the N/O abundance ratio, entail a third dredge-up episode.

The central star temperature varies from 296,000 K in region E to 197,000 K in region NE. This discrepancy is probably connected to differences in the optical depth, i.e., region E is not optically thick ([O II] 3727 is weaker in this region) and the corresponding temperature is an overestimate of the real effective temperature of the central star. Thus, a value around 200,000 K is probably closer to the real temperature of the PNN. This still is a factor ~ 3 larger than previous estimates (Glushkov et al. 1975; Kaler 1983b). But notice that the low temperatures ($\sim 70,000$ K) reported in these works are inconsistent with models for the PNN of type I PNe, since the central star will attain this temperature when it is about 500,000 yr old (Vassiliadis & Wood 1994; Blöcker 1995). The presence of the optical nebula proves that this is impossible.

Images of the central part of Sh 2-71 in [N II] 6584, [N II] 6584/H α , H 2 , and cK are displayed

in Figure 14. The binary system that includes the exciting star of the PN is at the center. Notice that the [N II] 6584/H α ratio is very small in the central “keyhole” cavity of this bipolar nebula, whose boundaries are sharply defined in this image. The spectral and morphological features of Sh 2-71 suggest that the H 2 image is a depiction of the distribution of molecular hydrogen in this object. Other evidence clearly indicates that this not so: Josselin et al. (2000) did not detect CO in Sh 2-71, and the main features observed in the H 2 frame (particularly the filament that extends to the west of the cavity) are replicated in a He I 5876 image (not shown) of Sh 2-71, a clear indication that emission from the He I lines at 2.11 μm dominates the infrared image. The absence of H 2 in the inspected region implies that either this is to be found in the external parts of Sh 2-71 or that the photodissociation front has had time enough to destroy all the molecular gas, i.e., that Sh 2-71 is sufficiently old (as suggested by these images). The central star temperature (close to 200,000 K) and the condition that Sh 2-71 is an old PN imply a large mass for the PNN and, consequently, for the progenitor star. For instance, the temperature of a 0.696 M_{\odot} PNN (from a 4 M_{\odot} progenitor) is less than 200,000 K after a thousand years, but this is the temperature of a 0.94 M_{\odot} PNN (from a 7 M_{\odot} progenitor) after 20,000 yr (Blöcker 1995).

Images of Sh 2-71 (with a larger field of view than in Figure 14) in [N II] 6584, [O III] 5007/H α (corrected for reddening), $C(\text{H}\beta)$ and $T(\text{N}^+)$ are shown in Figure 15. The temperature image was derived from a [N II] 6584 over [N II] 5755 image ratio, and relative values in the temperature image are accurate at the 30% level. A 3 \times 3 median filter was applied to reduce noise. The [O III] 5007/H α and $C(\text{H}\beta)$ images have the same accuracy and were filtered in the same way. The $C(\text{H}\beta)$ frame shows a global extinction pattern in the nebula (as in NGC 6302, Bohigas 1994): $C(\text{H}\beta) \sim 0.8 - 0.9$ to the E of the exciting star, and is consistently larger than unity (and up to ~ 1.5) to the N and NW. This contrast is also observed in the [O III] 5007/H α and $T(\text{N}^+)$ images: higher values of [O III] 5007/H α and $T(\text{N}^+)$ are found in the eastern lobe ([O III] 5007/H α is between 1 and 1.3 and $T(\text{N}^+) \simeq 11,000 - 13,000$ K) than in the northern and western regions (where [O III] 5007/H α < 1 and $T(\text{N}^+) \simeq 10,000$ K). The western filament that is so visible in the [N II] 6584 and H 2 images is very prominent in [O III] 5007/H α , since this ratio attains its minimum value (~ 0.5) along it. Finally,

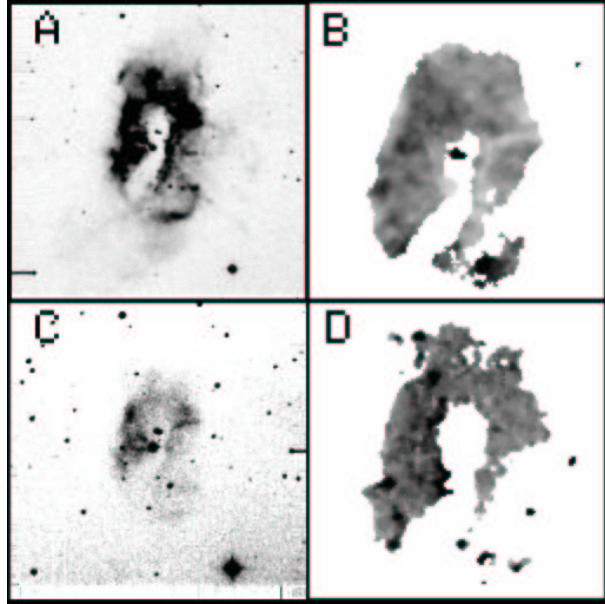


Fig. 15. Sh 2-71: (A) [N II] 6584, (B) [O III] 5007/H α (corrected for reddening), (C) C(H β), and (D) nitrogen temperature map. The FOV is 256'' \times 256'' in frames (A) and (C), 128'' \times 128'' in (B) and (D). North is up, east is to the left.

an electron density map of the same region covered by the temperature map does not display the aforementioned global structure (it was obtained from a [S II] 6724 to [S II] 6731 image ratio, but it is not shown): the electron density is very uniform ($\sim 400 \pm 100 \text{ cm}^{-3}$).

n) We 1-4

In this object the slit was not centered on a bright region (see Figure 16) and this had several consequences: [OII] 3727 was not detected and the oxygen abundance had to be assumed, [OIII] 4363 was not measured and $T(\text{O}^{+2})$ was supposed to be 1000 K larger than $T(\text{N}^+)$, and there were problems with sky subtraction close to He I 5876 so that He I 6678 was used to determine the He $^+$ concentration. In spite of all these it can be established with a large degree of confidence that We 1-4 is a type I PN, since He/H = 0.173 (0.254 when He I 5876 is used!) and the nitrogen lines are so strong that they necessarily lead to a large nitrogen overabundance (N/O = 1.11 with all these assumptions). Images of We 1-4 in [N II] 6584, [N II] 6584/H α , H 2 , and [O III] 5007 are shown in Fig. 16. The bipolar structure and the confining ring, inclined towards the line of sight, are very well defined, and leave little doubt that there is abundant shock-excited H 2 . It is worth noticing

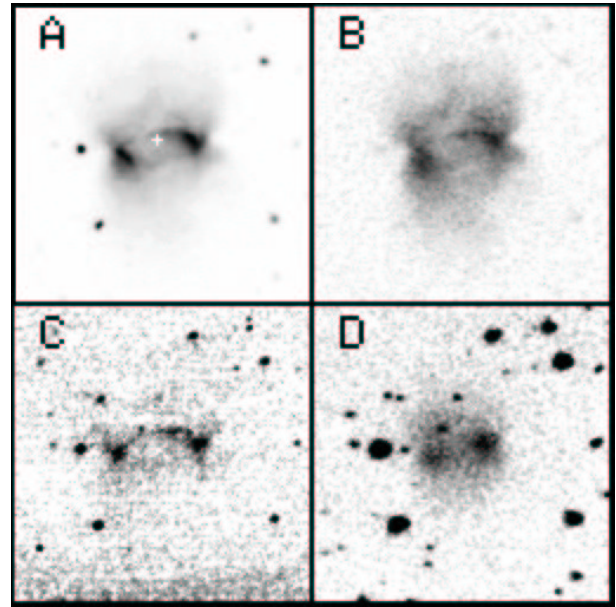


Fig. 16. We 1-4: (A) [N II] 6584, (B) [N II] 6584/H α , (C) H 2 , and (D) [O III] 5007. The position where the spectrum was taken is marked by a cross in (A). The FOV is 110'' \times 110''. North is up, east is to the left.

that Kastner et al. (1996), with a shorter integration time, failed to detect molecular hydrogen emission from We 1-4.

4. CONCLUSIONS

(1) The two primary criteria (He/H ≥ 0.125 and N/O ≥ 0.5) defining type I PNe (Peimbert 1978) are fulfilled in the following objects: BV 5-1, K 3-72, K 3-94, K 4-55, M 1-41, M 1-75, M 2-52, Sh 2-71, and We 1-4. With the exception of Sh 2-71, all these objects exhibit extensive evidence of shocked molecular hydrogen. In several cases H 2 was found to be further away from the geometrical center of the PN than the region where [N II] 6584 emission is brighter. In the case of Sh 2-71, it is possible that H 2 is located in the periphery, or that the photodissociation front has destroyed all the molecular gas, in which case it would follow that this PN was produced by a very massive progenitor.

(2) The chemical composition of JnEr 1 indicates that this nebula was produced by a relatively massive progenitor, as all type I PNe. This conclusion is not in agreement with its low N/O abundance ratio (0.39), though a much larger value (1.2) was reported in a previous work. This evolved nebula is apparently elliptical, though there is a hint that it may be a bipolar seen nearly pole-on. Line emission was observed through the H 2 filter, but it remains to

be established if it is from He I at 2.11 μm or from H_2 at 2.12 μm .

(3) The elliptical shape and probable absence of shocked molecular hydrogen in A 26 indicate that this is not a type I PN. Its helium abundance (≥ 0.125) combined with its N/O abundance ratio (0.28) does not match any of the types of PNe defined by Peimbert (1990).

(4) Shocked molecular hydrogen is probably present in K 3–92, a type IIb elliptical PN. This implies that K 3–92 must be a relatively young object, since the photodissociation front has not destroyed all the molecular gas.

(5) It is not certain if HDW 5 is an H II region or a type IIb PN. In either case, its bipolar morphology and the possible presence of shocked H_2 (suggested by the $H2$ image) are unexpected elements that need to be confirmed.

(6) The chemical composition of K 3–72, K 4–55, M 1–75, and Sh 2–71 implies that third dredge-up episodes occurred in their progenitor stars. The large temperatures found for the PNN of K 4–55, M 1–75, and Sh 2–71 are consistent with this conclusion, since they imply very massive progenitors. On the other hand, their spectra may be affected by shock waves (see below), casting some doubts on their abundances. This is not the case in K 3–72, where the most extreme abundances were determined, though the temperature of its central star does not suggest an exceptionally massive ZAMS progenitor ($3.5 M_{\odot}$ at the most).

(7) Large $T(\text{O}^{+2})/T(\text{N}^{+})$ ratios combined with small values for $\text{H}\alpha/[\text{S II}] 6724$ were observed in BV 5–1, K 4–55, M 1–41, M 1–75, and Sh 2–71 (see Table 5). This combination was interpreted as evidence for the presence of shock waves in the inspected regions. This does not necessarily apply to the entire nebula, as shown by Bohigas (1994) in the case of NGC 6302. Larger values of $T(\text{O}^{+2})/T(\text{N}^{+})$ are usually associated to small $\text{H}\alpha/[\text{S II}] 6724$ ratios (see Table 5), a combination that is usually found in shock-excited plasmas.

I would like to dedicate this work to two recently deceased friends and fellow workers: Víctor García and Pedro Ripa. They will be missed. The staff of San Pedro Mártir provided excellent assistance. Partial support from DGAPA-UNAM project IN-104991 is acknowledged.

REFERENCES

- Acker, A., Köpen, J., Stenholm, B., & Raytchev, B. 1991, *A&AS*, 89, 237 (AKSR)

- Acker, A., James, M., Ochsenbein, F., Stenholm, B., & Tylenda, R. 1992, *Strasbourg-ESO Catalogue of Planetary Nebulae*
- Ali, A., & Pfeiderer, J. 1999, *A&A*, 351, 1036 (AP)
- Aller, L. H. 1984, *Physics of Thermal Gaseous Nebula* (Dordrecht: Reidel)
- Aller, L. H., & Keyes, C. D. 1987, *ApJS*, 65, 405 (AK)
- Balick, B. 1987, *AJ*, 94, 671
- Bohigas, J. 1994, *A&A*, 288, 617
- _____. 1998, *RevMexAA*, 34, 87
- Blöcker, T. 1995, *A&A*, 299, 755
- Burton, M. G. 1992, *Aust. J. Phys.* 45, 463
- Cahn, J. A., Kaler, J. B., & Stanghellini, L. 1992, *A&AS*, 94, 399
- Cruz-González, I., et al. 1994, *Astronomical Instrumentation*, Proc. of SPIE, Vol. 8, 199
- Cuesta, L., & Phillips, J. P. 1993, *A&A*, 270, 379
- Dopita, M. A. 1977, *Ap&SS*, 48, 437 (D)
- Faúndez-Abans, M., & Maciel, W. J. 1987, *A&A*, 183, 324
- García-Segura, G., Langer, N., Różycka, M., Franco, J., & MacLow, M. 1998, *RevMexAASC*, 7, The Sixth Texas-Mexico Conference on Astrophysics: Astrophysical Plasmas — Near and Far, eds. R. J. Dufour & S. Torres-Peimbert (México, D. F.: Inst. Astron., UNAM), 50
- Glushkov, Y. I., Denisyuk, E. K., & Karyagina, Z. V. 1972, *Astron. Tsirk.*, 852, 3
- Guerrero, M. A., Manchado, A., & Serra-Ricart, M. 1996, *ApJ*, 456, 651 (GMS)
- Guerrero, M. A., Stanghellini, L., & Manchado, A. 1995, *ApJ*, 444, L49 (GSM)
- Guerrero, M. A., Villaver, E., Manchado, A., García-Lario, P., & Prada, F. 2000, *ApJS*, 127, 125
- Hora, J. L., Latter, W. B., & Deutsch, L. K. 1999, *ApJS*, 124, 195
- Huggins, P. J., Bachiller, R., Cox, P., & Forveille, T. 1996, *A&A*, 315, 284
- Iben, I. 1995, *Phys. Reports*, 250, 1
- Josselin, E., Bachiller, R., Manchado, A., & Guerrero, M. A. 2000, *A&A*, 353, 363
- Kahn, F. D. 1983, in *IAU Symp. 103, Planetary Nebulae*, ed. D. R. Flower (Dordrecht: Reidel), 305
- Kaler, J. B. 1983a, in *IAU Symp. 103, Planetary Nebulae*, ed. D. R. Flower, (Dordrecht: Reidel), 245
- _____. 1983b, *ApJ*, 271, 188
- Kaler, J. B., Chu, Y-H, & Jacoby, G. H. 1988, *AJ*, 96, 1407 (KCJ)
- Kaler, J. B., & Jacoby, G. H. 1989, *ApJ*, 345, 871
- Kaler, J. B., Kwitter, K. B., Shaw, R. A., & Browning, L. 1996, *PASP*, 108, 980 (KKSB)
- Kaler, J. B., Shaw, R. A., & Kwitter, K. B. 1990, *ApJ*, 359, 392 (KSK)
- Kastner, J. H., Weintraub, D. A., Gatley, I., Merrill, K. M., & Probst, G. 1996, *ApJ*, 462, 777 (Kas)
- Kingdon, J., & Ferland, G. J. 1995, *ApJ*, 442, 714
- Kingsburgh, R., & Barlow, M. J. 1994, *MNRAS*, 271, 257
- Kohoutek, L. 1979, *IBVS*, 1672, 1

- Kwok, S. 1982, *ApJ*, 258, 280
- Latter, W. B., Kelly, D. M., Hora, J. L., & Deutsch, L. K. 1995, *ApJS*, 100, 159
- Liebert, J., Fleming, T. A., Green, R. F., & Grauer, A. D. 1988, *PASP*, 100, 187
- Luhman, K. L., & Rieke, G. H. 1996, *ApJ*, 461, 298
- Manchado, A., Guerrero, M. A., Stanghellini, L., & Serra-Ricart, M. 1996, *The IAC Morphological Catalog of Northern Galactic Planetary Nebulae*, Instituto de Astrofísica de Canarias (IAC-Catalog)
- Méndez, R. H. 1991, in *IAU Symp. 145, Evolution of Stars: the Photospheric Abundance Connection*, eds. G. Michaud & A. Tutukov (Dordrecht: Kluwer), 375
- Peimbert, M. 1987, *Planetary and Proto-Planetary Nebulae: from IRAS to ISO*, ed. A. Preite-Martínez (Dordrecht: Reidel), 91
- _____. 1990, *Rep. Prog. Phys.* 53, 1559
- Peimbert, M., Sarmiento, A., & Fierro, J. 1991, *PASP*, 103, 815
- Peimbert, M., & Torres-Peimbert, S. 1983, in *IAU Symp. 103, Planetary Nebulae*, ed. D. R. Flower (Dordrecht: Reidel), 233
- Phillips, J. P. 1998, *A&A*, 340, 527
- Phillips, J. P., & Guzmán, V. 1998, *A&AS*, 130, 465
- Pottasch, S. R. 1983, in *IAU Symp. 103, Planetary Nebulae*, ed. D. R. Flower (Dordrecht: Reidel), 391
- Preite-Martínez, A., Acker, A., Köpen, J., & Stenholm, B. 1991, *A&AS*, 88, 121
- Różyczka, M., & Franco, J. 1996, *ApJ*, 469, 127
- Sabbadin, F. 1986, *A&A*, 160, 31
- Sabbadin, F., Falomo, R., & Ortolani, S. 1987, *A&AS*, 67, 541 (SFO)
- Sahai, R., & Bieging, J. H. 1993, *AJ*, 105, 595
- Schönberner, D. 1981, *A&A*, 103, 119
- Seaton, M. J. 1979, *MNRAS*, 187, 73P
- Stasińska, G., & Tylenda, R. 1990, *A&A*, 240, 467
- Sun, J., Sun Y-c., Lu, J., & Sun, J-j. 1998, *Acta Astron. Sinica*, 18, 217
- Vassiliadis, E., & Wood, P. R. 1994, *ApJS*, 92, 125
- Zazueta, S., et al. 2000, *RevMexAA*, 36, 141
- Zhang, C. Y. 1995, *ApJS*, 98, 659
- Zhang, H., Sun, J., & Ping, J. 2000, *Chinese AA*, 24, 309
- Zijlstra, A., Pottasch, S., & Bignell, C. 1990, *A&AS*, 82, 273
- Zuckerman, B., & Gatley, I. 1988, *ApJ*, 324, 501